ELECTRONIC STRUCTURE OF GRAPHENE NANO-RIBBONS

A THESIS

SUBMITTED TO THE DEPARTMENT OF PHYSICS

AND THE INSTITUTE OF ENGINEERING AND SCIENCE

OF BILKENT UNIVERSITY

IN PARTIAL FULFILLMENT OF THE REQUIREMENTS

FOR THE DEGREE OF

MASTER OF SCIENCE

By

Hüseyin Şener Şen

September, 2008

I certify that I have read this thesis and that in my opinion it is fully adequate, in scope and in quality, as a thesis for the degree of Master of Science.

Assoc. Prof. Dr. Oğuz Gülseren (Supervisor)

I certify that I have read this thesis and that in my opinion it is fully adequate, in scope and in quality, as a thesis for the degree of Master of Science.

Assist. Prof. Dr. M. Özgür Oktel

I certify that I have read this thesis and that in my opinion it is fully adequate, in scope and in quality, as a thesis for the degree of Master of Science.

Assist. Prof. Dr. Erman Bengü

Approved for the Institute of Engineering and Science:

Prof. Dr. Mehmet B. Baray
Director of the Institute Engineering and Science

ABSTRACT

ELECTRONIC STRUCTURE OF GRAPHENE NANO-RIBBONS

Hüseyin Şener Şen
M.S. in Physics
Supervisor: Assoc. Prof. Dr. Oğuz Gülseren
September, 2008

Graphite is a known material to human kind for centuries as the lead of a pencil. Graphene as a two dimensional material, is the single layer of graphite. Many theoretical works have been done about it so far, however, it newer took attention as it takes nowadays. In 2004, Novoselov et al. was able to produce graphene in 2D. Now that, making experiments on graphene is possible scientists have to renew their theoretical knowledge about systems in two dimension because graphene, due to its electronic structure, is able to prove the ideas in quantum relativistic phenomena. Indeed, recent theoretical studies were able to show that, electrons and holes behave as if they are massless fermions moving at a speed about 10^6m/s (c/300, c being speed of light) due to the linear electronic band dispersion near K points in the brillouin zone which was observed experimentally as well.

Having zero band gap, graphene cannot be used directly in applications as a semiconductor. Graphene Nano-Ribbons (GNRs) are finite sized graphenes. They can have band gaps differing from graphene, so they are one of the new candidates for band gap engineering applications such as field effect transistors. This work presents theoretical calculation of the band structures of Graphene Nano-Ribbons in both one (infinite in one dimension) and zero dimensions (finite in both dimensions) with the help of tight binding method. The calculations were made for Zigzag, Armchair and Chiral Graphene Nano-Ribbons (ZGNR,AGNR,CGNR) in both 1D and 0D. Graphene nano-ribbons with zero band gap (ZGNR and AGNR) are observed in the calculations as well as the ribbons with finite band gaps (AGNR and CGNR) which increase with the decrease in the size of the ribbon making them much more suitable and strong candidate to replace silicon as a semiconductor.

Keywords: Graphene, nano-ribbon, tight binding, electronic structure, hydrogen saturation of dangling bonds, band gap, AGNR, ZGNR, CGNR, 1D, 0D, quantum confinement, chiral angle, chiral vector..

ÖZET

GRAFİN NANO-ŞERİTLERİN ELEKTRONİK YAPISI

Hüseyin Şener Şen
Fizik, Yüksek Lisans
Tez Yöneticisi: Doç. Dr. Oğuz Gülseren
Eylül, 2008

İnsanların yüzyıllardır kalem ucu olarak kullandığı grafit katmanlardan oluşmaktadır ve her bir katmana grafin denir. 2004 yılında Novoselov ve ekibi iki boyutlu grafini üretmeyi başardı. Daha önce grafin üzerine epeyce teorik çalışma yapılmıştı ve bu yeni gelişme deneysel çalışmalara da imkan sağladı. Yapılan çalışmalar gösteriyor ki grafin, elektronik yapısı sebebiyle, kuvantumsal görelilikçe ortaya atılan fikirleri doğruluyor. Bu sebeple bilim adamları iki boyutlu sistemler hakkındaki düşüncelerini tekrar gözden geçirmek zorunda kaldılar. Hatta son yapılan teorik çalışmalar, deneysel verileri doğrular şekilde gösteriyor ki, elektronlar ve deşikler brillouin bölgesi içindeki K noktası civarında oluşan konik elektronik bant dağılımı sebebiyle 10^6m/s hızla hareket eden (c/300, c ışık hızı) kütlesiz fermiyonlar gibi davranıyorlar.

Grafinin bant aralığı sıfır olduğundan yarı iletken uygulamalarında kullanılamamaktadır. Grafin nano-şeritler (GNŞ) sonlu büyüklükteki grafinlerdir. Grafinden farklı olarak bant aralıkları sıfır olmayabilir, bu nedenle bant aralığı mühendisliği uygulamaları için (mesela transistörler) yeni bir adaydır. Bu çalışma zayıf bağlanma yöntemiyle hem bir boyutlu (bir boyutta sonsuz), hem de sıfır boyutlu (iki boyutta da sonlu) Grafin Nano-Şeritlerin elektronik bant yapısının hesaplanmasını sunuyor. Hesaplamalar hem bir boyutta, hem de sıfır boyutta Zigzag, Koltuk ve Kiral Grafin Nano-Şeritler (ZGNŞ, KGNŞ, KiGNŞ) için yapıldı. Hesaplar, grafindeki gibi sıfır bant aralıklı grafin nano-şeritlerin (ZGNŞ ve KGNŞ) olduğunu gösterdiği gibi, bant aralığı boyutları küçüldükçe artan ve böylece silikonun yerini almak için daha uygun ve güçlü bir aday haline gelen sıfırdan farklı bant aralığına sahip (KGNŞ ve KiGNŞ) grafin nano-şeritlerin de varlığını göstermektedir.

Anahtar sözcükler: Grafin, nano-şerit, zayif baglanma, elektronik yapı, hidrojenle doyurma, bant aralığı, KGNŞ, ZGNŞ, 1 boyutlu, 0 boyutlu, kiral açı, kiral vektör.

Acknowledgement

I would like to express my gratitude to my supervisors Assoc. Prof. Dr. Oğuz Gülseren for his instructive comments in the supervision of the thesis.

I would like to express my special thanks and gratitude to Assist. Prof. Dr. M. Özgür Oktel and Assist. Prof. Dr. Erman Bengü for showing keen interest to the subject matter and accepting to read and review the thesis.

I would like to thank my friends Pınar Pekçağlıyan (Çolak), Recep Çolak, Abdurrahman Bulut, Rasim Yurtcan, Yunus Yılmaz, Aykut Şahin, Ümit Aslan, Cüneyt Öztürk, Ceyda Sanlı, Ömer Hamdi Kaya, Ersoy Yıldırım, Okan Dilek, and Ali Burak Kurtulan (AgA) for their invaluable friendship and support.

I would like to thank to my parents Ahmet-Necla Şen and brothers Şenol-İbrahim Şen for their great efforts to help me overcome any difficulties throughout my life.

I would like to thank to my mother-in-law Hüsne Soyer and sister-in-law Derya Soyer.

Finally, I would like to thank to my beloved wife Hicran Şen for everything she done for us.

Contents

List of Figures

List of Tables

Chapter 1

Introduction

Carbon is one of the basic element which is extremely important for life on earth. Only by looking at the role in organic chemistry, carbon can be declared as the most important element on earth. Since it has flexibility in bonding like sp, sp^2 or sp^3; many compounds including carbon show very different geometrical and electronic structures and properties. For a physicist dealing with nano-sized structures, geometry of the structure is greatly important, since it determines the dimensionality [1]. (See the figure 1.1)

Graphene, for instance, is only made up of carbon atoms which is two dimensional (2D), whereas carbon nanotube is a one dimensional (1D) material. The dimensions, of course, affect most of the physical properties of the material. In graphene, carbon atoms create a honeycomb structure with hexagons on a plane. In carbon nanotubes these hexagons are not planar but they are rolled to create a cylinder. In fullerenes, however, the structure is just a sphere, which makes them zero dimensional (0D) molecules with discrete energy states. Graphite, is a three dimensional (3D) allotrope of carbon, which is known for centuries. They are made out of stacks of graphene layers which are weakly bound by van der Waals forces. Therefore, graphite can be expected to have closer physical properties to graphene. Theoretical works enlighten these expectations, however, experimental works can recently be done since graphene could not be obtained as a single layer until 2004 [2]. After this date, the importance of graphene once more realized

and many researchers started to examine it again.

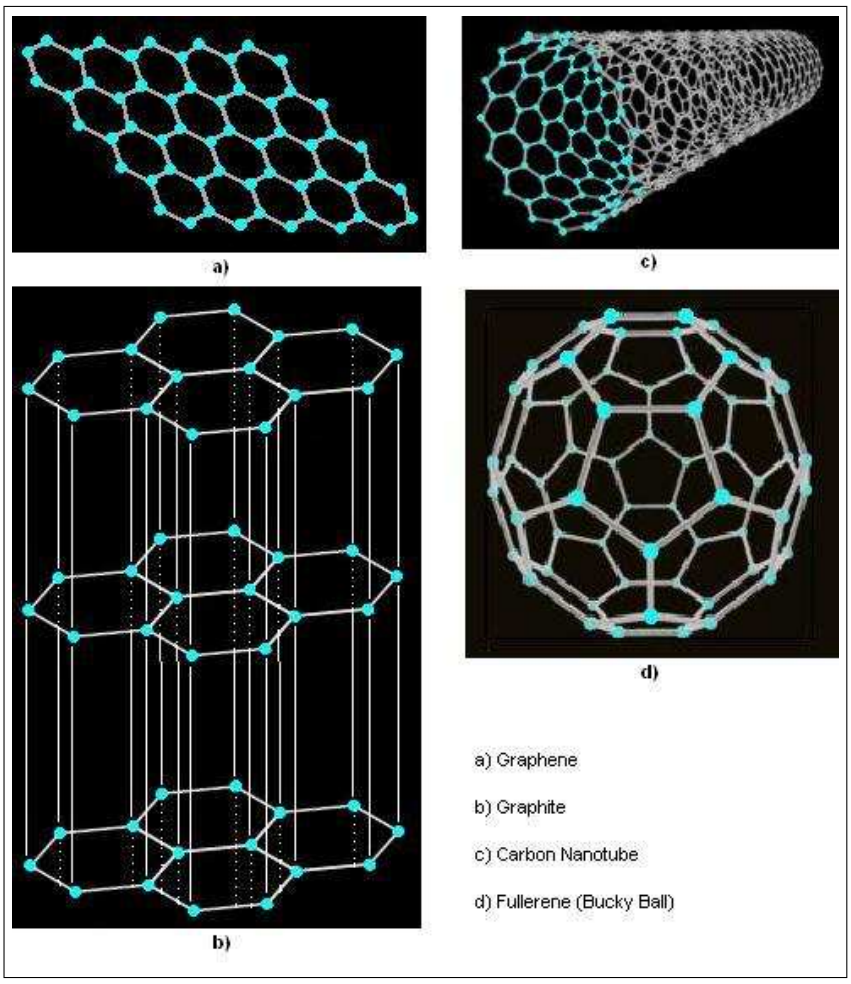

Figure 1.1: Structures of Carbon with different dimensions. a) Graphene consists of honeycomb lattice of carbon atoms in 2D, b) Graphite is a stack of graphene layers creating a 3D structure, c) Carbon Nanotubes are rolled-up cylinders of graphene in 1D and d) Fullerenes (C_{60}) are molecules consisting of wrapped graphene by introduction of pentagons on honeycomb lattice in 0D. Graphene is mother of them all.

Graphene nano-ribbons are structures with a rectangular shape which are cut from graphene sheet. Since they have finite width and length, in nano scale, they are considered to be 0D structures. They can have different physical properties depending on their width, length and chirality. If we consider the length to be

infinite, they become 1D structure [3,4]. There are theoretical works in the literature on both 1D and 0D graphene nano-ribbons, however, they mostly consider either very small width and length to have a small number of carbon atoms included, which cannot be created experimentally for quite long time, or ribbons with large width but infinitely long length which is not what is aimed. There is even no work in the literature that deals with chirality of the ribbons. This work presents the electronic structure of graphene nano-ribbons with large width and finite length. Also, the chiral nano ribbons are also included. The calculations are made by using tight binding method. The reason to use tight binding method is that it is fast and reliable for this calculation, and it can deal with many atoms at once, which other methods cannot.

1.1 Tight Binding Method

The tight-binding (TB) model is a kind of counterpart of the nearly-free electron approximation. The approximation of the TB method assumes that the restricted Hilbert space, spanned by atomic-like orbitals is sufficient to describe the wave functions solution of the Schrodinger equation (at least in restricted energy range). Such an atomic-like basis provides a natural, physically motivated description of electronic states in matter [5]. In tight binding calculations, due to the translational symmetry, any wave function should satisfy the Bloch's Theorem [5]

$$T_{\vec{a}_i}\Psi = e^{i\vec{k}\cdot\vec{a}_i}\Psi \tag{1.1}$$

where T_{a_i} is a translational operation along the lattice vector $\vec{a_i}$ $(i = 1, 2, 3)$, and $\vec{k}$ is the wave vector. For the purpose, we define $\Phi(\vec{k}, \vec{r})$ as a Tight Binding Bloch function which is given by [5]

$$\Phi_j(\vec{k}, \vec{r}) = \frac{1}{\sqrt{N}} \sum_{\vec{R}}^{N} e^{i\vec{k}\cdot\vec{R}} \psi_j(\vec{r} - \vec{R}),\ (j = 1, ..., n). \tag{1.2}$$

$\vec{R}$ is the position of the atom and ψ_j denotes the atomic wave function in state j, N is the number of unit cells, n is the number of Bloch functions in the solid for a given $\vec{k}$. From equation 1.2, it is clear that $\Phi_j(\vec{k}, \vec{r} + \vec{a}) = e^{i\vec{k}\cdot\vec{a}}\ \Phi_j(\vec{k}, \vec{r})$ so

$T_{Ma_i} = 1$ which also expresses $e^{ikMa_i} = 1$ [5]. Then the wave number k is equal to $2p\pi/Ma_i$ where $p = 0, 1, 2, ..., M-1$, $i = 1, 2, 3$. The eigenfunctions in the solid $\Psi_j(\vec{k}, \vec{r})$ are expressed by a linear combination of Bloch functions as follows;

$$\Psi_j(\vec{k}, \vec{r}) = \sum_{j'=1}^{n} C_{jj'}(\vec{k})\Phi_{j'}(\vec{k}, \vec{r}). \tag{1.3}$$

Here, $C_{jj'}$ are coefficients to be determined. The j'th eigenvalue as a function of $\vec{k}$ is given by;

$$E_j(\vec{k}) = \frac{\langle \Psi_j | H | \Psi_j \rangle}{\langle \Psi_j | \Psi_j \rangle} \tag{1.4}$$

where H is the hamiltonian of the solid. Substituting equation 1.3 into equation 1.4, we obtain;

$$E_i(\vec{k}) = \frac{\sum_{j,j'=1}^{n} H_{jj'}(\vec{k}) C_{ij}^* C_{ij'}}{\sum_{j,j'=1}^{n} S_{jj'}(\vec{k}) C_{ij}^* C_{ij'}} \tag{1.5}$$

where the integrals over the Bloch orbitals, $H_{jj'}(\vec{k}) = \langle \Phi_j | H | \Phi_{j'} \rangle$ and $S_{jj'}(\vec{k}) = \langle \Phi_j | \Phi_{j'} \rangle$ $(j, j' = 1, ..., n)$ are called transfer integral matrices and overlap integral matrices respectively. If we minimize the eigenvalue by taking derivative with respect to C_{ij}^* and use it in equation 1.5, we have the generalized eigenvalue equation

$$HC_i = E_i(\vec{k}) S C_i, \tag{1.6}$$

where C_i is defined as a column vector with elements $C_{i1}, ..., C_{iN}$. By transporting the right hand side to the left we have either $C_i = 0$, which represents the null vector, or secular equation as follows;

$$det|H - ES| = 0. \tag{1.7}$$

By solving the secular equation, one can have the eigenvalues which are energy values $E_i(\vec{k})$, $(i = 1, ..., n)$ for a given $\vec{k}$ [5].

1.2 Electronic Properties of Graphene

Graphene can be defined as single layer of graphite. Although it is a 2D material the electronic structure does not differ much from graphite. This is because

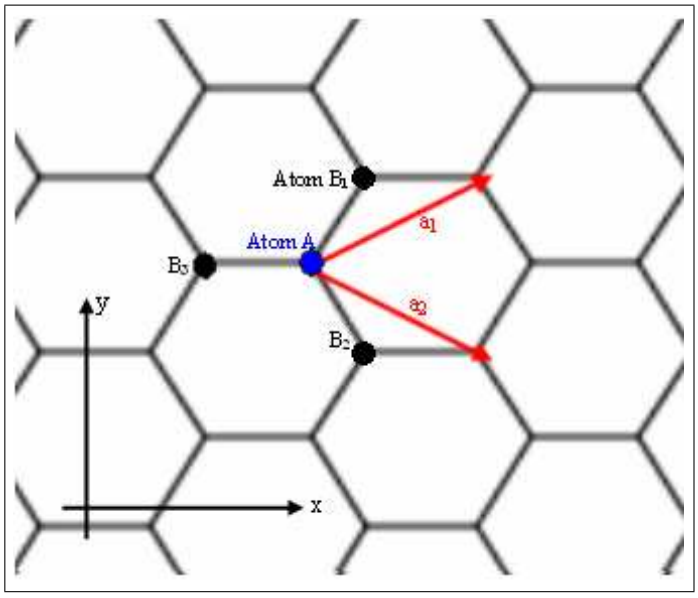

Figure 1.2: Carbon atoms are located at the corners of the hexagons. Blue dot shows A type and black dots show three nearest B type atoms. Red arrows are lattice vectors $\vec{a}_1$ and $\vec{a}_2$

even for graphite, interactions between the layers are very weak since layer to layer distance is 3.35 Å, which is more than twice the interatomic bond distance between carbon atoms in the single layer. Graphite has been known by human kind since 1564, the invention of pencil. Although it is known for 444 years, the experimentalists have recently been able to investigate one atom thick flakes among the pencil debris [1]. Therefore, single layer of graphite could be isolated in 2004.

In graphene, carbon makes sp^2 hybridization. One s orbital (one 2s orbital) combines with two p orbitals (two 2p) which leads a trigonal planar structure. Carbons make σ bonds with each other. They are separated with a distance of 1.42 Å. If we put graphene layers one above another there occurs a π bond between them leading to the formation of graphite. Last remaining electron in 2p orbital is responsible for this π bond which is not related to sp^2 hybridization. Since in graphene there is an unaffected p orbital perpendicular to the planar structure, each carbon has one extra electron and π band is half filled.

With tight binding approach, electronic structure of graphene can be examined and explained very easily. Since carbon atoms make hexagonal structure, it can be seen as a triangular lattice. If we choose the distance between carbon atoms as a, the lattice vectors can be written as [1];

$$\vec{\mathbf{a}}_{\mathbf{1}} = \frac{a}{2}(3, \sqrt{3}) \tag{1.8}$$

$$\vec{\mathbf{a}}_{\mathbf{2}} = \frac{a}{2}(3, -\sqrt{3}). \tag{1.9}$$

If one generates a lattice with these lattice vectors to make a graphene, there are two atoms inside the unit cell, atom A and atom B. Both of these atoms are carbon atoms of course and there is no difference between them except for the definition of positions.

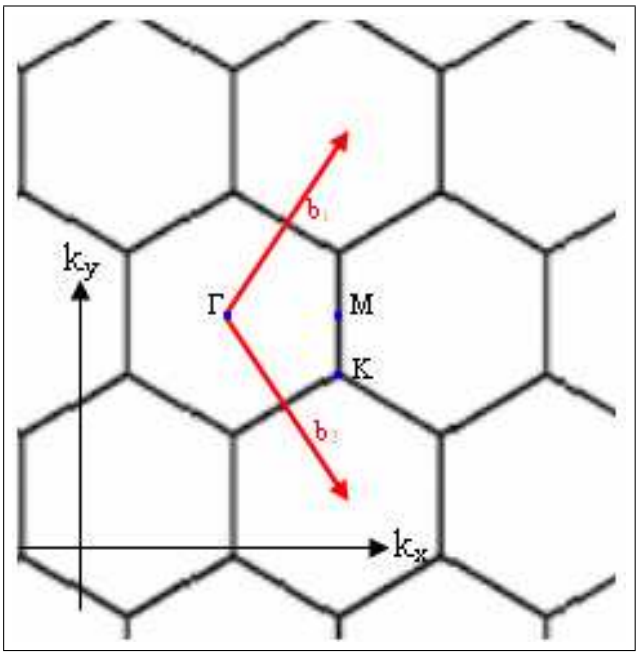

Figure 1.3: The corresponding reciprocal of graphene lattice shown in figure 1.2. High symmetry points Γ, K and M are indicated with blue dots and red arrows show the reciprocal lattice vectors.

By using these lattice vectors, reciprocal lattice vectors can be defined as;

$$\vec{\mathbf{b}}_{\mathbf{1}} = \frac{2\pi}{3a}(1, \sqrt{3}) \tag{1.10}$$

$$\vec{\mathbf{b}}_{\mathbf{2}} = \frac{2\pi}{3a}(1, -\sqrt{3}). \tag{1.11}$$

In the Brillouin zone of graphene, there are three special points, that ease the problem of determining the electronic structure. These points are so called high symmetry points which are Γ, K and M. The positions of these points in momentum space can be defined as (see figure 1.3);

$$\mathbf{\Gamma} = (0,0) \tag{1.12}$$
$$\mathbf{K} = (\frac{2\pi}{3a}, \pm\frac{2\pi}{3\sqrt{3}a}) \tag{1.13}$$
$$\mathbf{M} = (\frac{2\pi}{3a}, 0). \tag{1.14}$$

Putting atom A at the origin in real space the three nearest neighbours are located at;

$$\delta_{\mathbf{1}} = \frac{a}{2}(1,\sqrt{3}) \tag{1.15}$$
$$\delta_{\mathbf{2}} = \frac{a}{2}(1,-\sqrt{3}) \tag{1.16}$$
$$\delta_{\mathbf{3}} = a(-1,0). \tag{1.17}$$

δs are the positions of B atoms, since they are the nearest neighbours of atom A. The six second nearest neighbours for the atom A are positioned at;

$$\delta'_{\mathbf{1}} = \frac{a}{2}(3,\sqrt{3}) \tag{1.18}$$
$$\delta'_{\mathbf{2}} = \frac{a}{2}(3,-\sqrt{3}) \tag{1.19}$$
$$\delta'_{\mathbf{3}} = a(0,-\sqrt{3}) \tag{1.20}$$
$$\delta'_{\mathbf{4}} = \frac{a}{2}(-3,-\sqrt{3}) \tag{1.21}$$
$$\delta'_{\mathbf{5}} = \frac{a}{2}(-3,\sqrt{3}) \tag{1.22}$$
$$\delta'_{\mathbf{6}} = a(0,\sqrt{3}). \tag{1.23}$$

To calculate the band structure of graphene by using tight binding method we have to construct the hamiltonian matrix H. For simplicity of explanation, first nearest neighbour approach can be used. Then, to calculate π bands there is only an integration over a single atom in H_{AA} and H_{BB}. Thus, H_{AA}=H_{BB}=ϵ_{2p} for the diagonal elements of 2x2 Hamiltonian matrix. For off diagonal elements, we

have to use first nearest neighbour positions as follows [5];

$$H_{AB} = t(e^{i\vec{k}\cdot\vec{\delta_1}} + e^{i\vec{k}\cdot\vec{\delta_2}} + e^{i\vec{k}\cdot\vec{\delta_3}}) = tf(k) \tag{1.24}$$

where t is the transfer integral between p orbitals of atom A and atom B, $\vec{k}$ is the wave vector that we consider and $f(k)$ is a function of the sum of the phase factors of $e^{i\vec{k}\cdot\delta_j}$ (j=1,2,3). Using x and y coordinates in figure 1.2, $f(k)$ is given by;

$$f(k) = e^{-ik_x a} + 2e^{ik_x a/2}\cos(k_y a\sqrt{3}/2). \tag{1.25}$$

Since $f(k)$ is a complex function and hamiltonian matrix should be hermitian, we write $H_{AB} = H^*_{AB}$, where $*$ denotes complex conjugate. Then, the Hamiltonian matrix can be written in matrix form as;

$$H = \begin{pmatrix} \epsilon_{2p} & tf(k) \\ tf(k)^* & \epsilon_{2p} \end{pmatrix}. \tag{1.26}$$

To solve the secular equation $det(H - ES) = 0$ we need the overlap matrix S. For this problem overlap matrix is the following;

$$S = \begin{pmatrix} 1 & sf(k) \\ sf(k)^* & 1 \end{pmatrix} \tag{1.27}$$

where s is the overlap integral that tells us about the quantity of the overlapping. Then, the eigenvalues of $E(\vec{k})$ can be obtained as a function of $\vec{k}$, t and s as shown in equation 1.28.

$$E(\vec{k}) = \frac{\epsilon_{2p} \pm t\sqrt{|f(\vec{k})|^2}}{1 \pm s\sqrt{|f(\vec{k})|^2}} \tag{1.28}$$

where + signs in both numerator and denominator go together to obtain bonding π energy band, whereas minus signs indicate the anti-bonding π band. Using $\epsilon_{2p} = 0$, $t = -3.033$eV, $s = 0.129$eV in equation 1.28, we can obtain the following energy dispersion relation graph, figure 1.4 [5]. When the overlap integral s becomes zero, the π and π^* bands become symmetric around $E = \epsilon_{2p}$.

$$E(\vec{k}) = \pm t\{1 + 4\cos(\frac{3k_x a}{2})\cos(\frac{k_y a\sqrt{3}}{2}) + 4\cos^2(\frac{k_y a\sqrt{3}}{2})\}^{1/2} \tag{1.29}$$

In this case the energies at Γ, K and M are $\pm 3t$, 0 and $\pm t$ respectively.

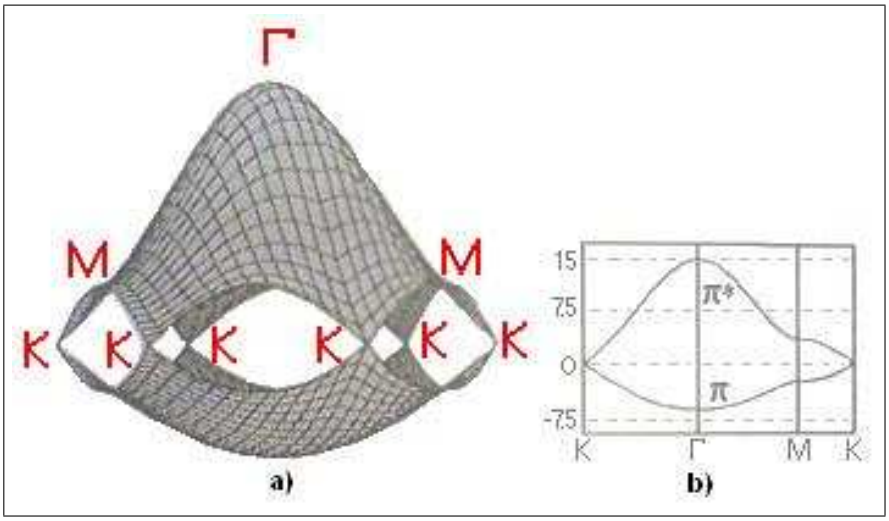

Figure 1.4: (a) The energy dispersion relations for graphene shown throughout the whole region of Brillouin zone. (b) The energy dispersion along the high symmetry directions of the triangle ΓMK. (Reproduced from G. Dresselhaus, M. S. Dresselhaus, and R. Saito, *Physical Properties of Carbon Nanotubes*, Imperial College Press, London, 1998.)

In order to calculate σ bonds of graphene we have to consider a 6x6 Hamiltonian matrix. This is because, now we have to deal with 3 hybrid sp^2 bonds. In fact, for the first nearest neighbour approximation many elements in the matrix are zero. New hamiltonian can be shown in the matrix form as;

$$H = \begin{pmatrix} \epsilon_{2s} & 0 & 0 & \langle 2s_A|2s_B\rangle & \langle 2s_A|2p_{xB}\rangle & \langle 2s_A|2p_{yB}\rangle \\ 0 & \epsilon_{2p} & 0 & \langle 2p_{xA}|2s_B\rangle & \langle 2p_{xA}|2p_{xB}\rangle & \langle 2p_{xA}|2p_{yB}\rangle \\ 0 & 0 & \epsilon_{2p} & \langle 2p_{yA}|2s_B\rangle & \langle 2p_{yA}|2p_{xB}\rangle & \langle 2p_{yA}|2p_{yB}\rangle \\ \langle 2s_B|2s_A\rangle & \langle 2s_B|2p_{xA}\rangle & \langle 2s_B|2p_{yA}\rangle & \epsilon_{2s} & 0 & 0 \\ \langle 2p_{xB}|2s_A\rangle & \langle 2p_{xB}|2p_{xA}\rangle & \langle 2p_{xB}|2p_{yA}\rangle & 0 & \epsilon_{2p} & 0 \\ \langle 2p_{yB}|2s_A\rangle & \langle 2p_{yB}|2p_{xA}\rangle & \langle 2p_{yB}|2p_{yA}\rangle & 0 & 0 & \epsilon_{2p} \end{pmatrix}. \tag{1.30}$$

Since it is a hermitian matrix, the eigenvalues, which are energy values, are real as it should be. To calculate the overlapping of the orbitals, we have to decompose the wavefunctions into its σ and π components along the relevant bond. For $|2s\rangle$ there is no such decomposition, however, $|2p_x\rangle$ has. As an example, we can calculate two elements [(1,5) and (3,5)] of the hamiltonian matrix. To calculate

(1,5), we need $\langle 2s_A|$ and three $|2p_{xB}\rangle$ from three nearest neighbours. Three bonds of atom A with B atoms have different directions, so we have to decompose $|2p_{xB}\rangle$ to σ and π components along the relevant bond. If we consider the atoms in figure 1.2, we can see that atom A makes bonds with B_1 and B_2 not along x direction, but is has an angle of $\pi/3$. We can decompose $|2p_{xB1}\rangle$ as follows;

$$|2p_x\rangle = \cos(\frac{\pi}{3})|2p_\pi\rangle + \sin(\frac{\pi}{3})|2p_\sigma\rangle. \tag{1.31}$$

For B_2 the same procedure is applied and it has the same decomposition for $|2p_x\rangle$. Then, we can calculate the value of (1,5) by the following equation;

$$\begin{aligned}\langle 2s_A|2p_{xB}\rangle &= \langle 2s|\{H_{sp\sigma}(-e^{ik_xa} + e^{ik_xa/2}e^{ik_ya\sqrt{3}/2}\sin(\pi/3) + e^{ik_xa/2}e^{-ik_ya\sqrt{3}/2}\sin(\pi/3))|2p_\sigma\rangle \\ &+H_{sp\pi}(e^{ik_xa/2}e^{ik_ya\sqrt{3}/2}\cos(\pi/3) + e^{ik_xa/2}e^{-ik_ya\sqrt{3}/2}\cos(\pi/3))|2p_\sigma\rangle\}. \end{aligned}\tag{1.32}$$

Here, $H_{sp\sigma}$ is the coupling parameter between $2s$ and $2p_\sigma$ of atom A and B. Similarly $H_{sp\pi}$ is the coupling parameter for $2s$ and $2p_\pi$ and it is equal to zero. Therefore, the last term in the equation above drops and we have only $H_{sp\sigma}$ which we call H_{sp} here after. For the calculation of the value of the element (3,5) in hamiltonian matrix, we need to decompose $\langle 2p_{yA}|$ just like we did for $|2p_{xB}\rangle$. In the direction of the bond to both B_1 and B_2, it can be decomposed as; $\langle 2p_x| = \sin(\pi/3)\langle 2p_\sigma| + \cos(\pi/3)\langle 2p_\pi|$. In the direction of the bond to B_3 we do not have to decompose it, since the bond is in the x direction and wavefunctions are perpendicular to each other resulting in zero overlapping. Then, the value of (3,5) can be calculated as;

$$\begin{aligned}\langle 2p_{yA}|2p_{xB}\rangle &= \{\sin(\pi/3)\langle 2p_\sigma| + \cos(\pi/3)\langle 2p_\pi|\} \\ &\{H_{pp\sigma}(-e^{ik_xa/2}e^{ik_ya\sqrt{3}/2}\cos(\pi/3) + e^{ik_xa/2}e^{-ik_ya\sqrt{3}/2}\cos(\pi/3))|2p_\sigma\rangle \\ &+H_{pp\pi}(-e^{ik_xa/2}e^{ik_ya\sqrt{3}/2}\sin(\pi/3) + e^{ik_xa/2}e^{-ik_ya\sqrt{3}/2}\sin(\pi/3))|2p_\sigma\rangle\} \\ &= -\frac{\sqrt{3}}{2}(H_{pp\sigma} + H_{pp\pi})e^{ik_xa/2}\cos(k_ya\sqrt{3}/2) \end{aligned}\tag{1.33}$$

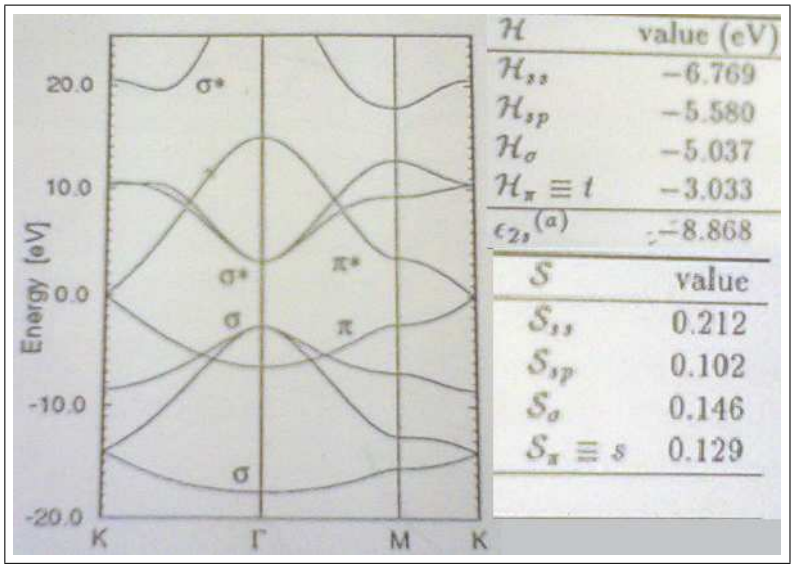

$\mathcal{H}$	value (eV)
$\mathcal{H}_{ss}$	−6.769
$\mathcal{H}_{sp}$	−5.580
$\mathcal{H}_{\sigma}$	−5.037
$\mathcal{H}_{\pi} \equiv t$	−3.033
$\epsilon_{2s}{}^{(a)}$	−8.868

$\mathcal{S}$	value
$\mathcal{S}_{ss}$	0.212
$\mathcal{S}_{sp}$	0.102
$\mathcal{S}_{\sigma}$	0.146
$\mathcal{S}_{\pi} \equiv s$	0.129

Figure 1.5: Graphene electronic band structure and the parameters used in calculation in Dresselhaus ($\epsilon_{2p} = 0$). (Adapted from G. Dresselhaus, M. S. Dresselhaus, and R. Saito, *Physical Properties of Carbon Nanotubes*, Imperial College Press, London, 1998.)

where $H_{pp\sigma}$ and $H_{pp\pi}$ are coupling parameters. After determining all of the elements of the Hamiltonian matrix, and choosing s=0 in overlap matrix, we can solve the secular equation and find out the energy values for all $\vec{k}$.

Energy bands of graphene is shown in figure 1.5 [5] by using the parameters of Dresselhaus. Although this graph is drawn by using nonzero s values in overlap matrix, it only uses first nearest neighbour approximation and does not deal with second nearest A type atoms. In our calculation, we used the parameters shown in table 1.1 [6] and included the second nearest neighbours. However, we assumed that overlap matrix is an identity matrix.

Using these parameters, the calculated band structure is shown in figure 1.6. Valance bands in figure 1.6 almost match with the valance bands given in figure 1.5 except for the two lowest σ bands in between M and K points. However, they do not effect the electronic structure much. In conduction band, however, the highest σ^* band seem to differ mostly. This is due to the approximation made for overlap matrix to be an identity matrix. The most important part of the band

Table 1.1: Tight binding coupling parameters for carbon (Adapted from D. Tomanek, S. G. Louie, Phys. Rev B **37**, 8327 (1988))

First nearest neighbour parameter	Value(eV)	Second nearest neighbour parameter	Value(eV)
ϵ_s	-7.3	H_{ss2}	-0.18
ϵ_p	0	H_{sp2}	0
H_{ss}	-4.30	$H_{pp\sigma 2}$	0.35
H_{sp}	4.98	$H_{pp\pi 2}$	-0.10
$H_{pp\sigma}$	6.38		
$H_{pp\pi}$	-2.66		

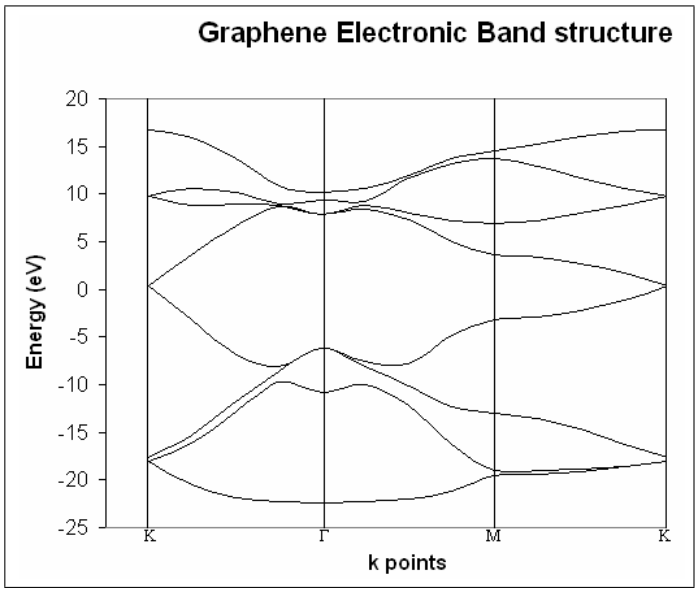

Figure 1.6: Graphene electronic band structure calculated by using tight binding parameters shown in table 1.1 and drawn between Γ, K and M points to compare with figure 1.5.

structure is π and π^* bands and they seem to match quite well. In both figures for band structure of graphene, the valance and the conduction bands touch at K points creating zero energy gap. This makes graphene a semi-metal. At these Dirac points, the dispersion is conical. Near these crossing points, the electron energy is linearly dependent on the wave vector and it is given by;

$$E_{\pm}(\mathbf{q}) \cong \pm v_F|\mathbf{q}| + \Theta(q^2) \tag{1.34}$$

where $\mathbf{q}$ is the momentum measured relatively to the Dirac points and v_F is the Fermi velocity [1]. According to Wallace [8], the value of this velocity is around $10^6\ m/s$, which is around $c/300$, c being the speed of light.

The energy spectrum of graphene resembles the energy of ultra-relativistic particles which are quantum mechanically described by the Dirac equation. A result of this Dirac like spectrum is, cyclotron mass. The cyclotron mass is defined as

$$m^* = \frac{1}{2\pi}\frac{\partial A(E)}{\partial E}, \tag{1.35}$$

where $A(E)$ is the area enclosed by orbit in momentum space. $A(E)$ is given by;

$$A(E) = \pi q^2 = \pi\frac{E^2}{v_F^2}. \tag{1.36}$$

Using 1.36 in 1.35, one can obtain

$$m^* = \frac{E}{v_F^2} = \frac{q}{v_F}. \tag{1.37}$$

The electronic density is related to the Fermi momentum as $n = k_F^2/\pi$ leading to the following equation;

$$m^* = \frac{\sqrt{\pi}}{v_F}\sqrt{n}. \tag{1.38}$$

Therefore, cyclotron mass depends on the square root of electronic density. The experimental data fits very well to the calculated results providing an estimation Fermi velocity around $10^6\ m/s$ [1]. The experimental observation for the dependence of cyclotron mass to $\sqrt{n}$, provides an evidence for the existence of massless Dirac quasi-particles in graphene.

According to Castro [1] the density of states is shown in figure 1.7 both for first and second nearest neighbour approximation. In both cases graphene shows

semi-metallic behaviour. According to the figures that zoom to Fermi level, the density of states changes linearly with energy, $\rho(\epsilon) \propto |\epsilon|$ [1].

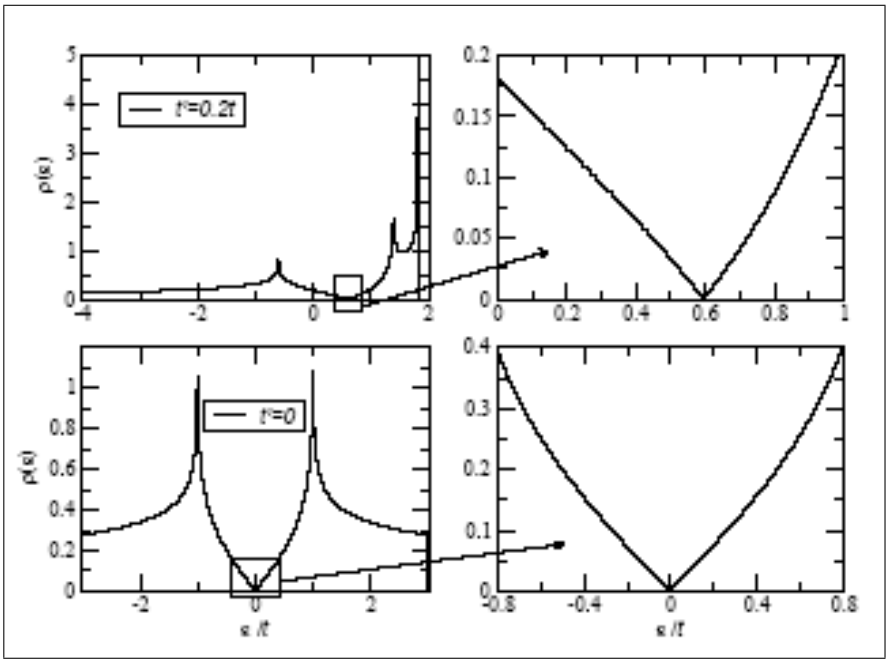

Figure 1.7: Density of states of graphene computed with second nearest neighbour (top) and first nearest neighbour approximation (bottom). Also shown on the right hand side is zoom in of the density of states close to the neutrality of one electron per site. (Taken from A. H. C. Neto, F. Guinea, N. M. R. Peres, K. S. Novoselov and A. K. Geim, arXiv:0709.1163, Rev. Mod. Phys. (to be published).)

1.3 Organization of the Thesis

The thesis consists of 4 chapters. First chapter is an introductory chapter which includes the motivation of this study and a brief information about graphene. The second chapter continues with the information, calculation, and the theoretical results about the band structure of graphene nano-ribbons (GNRs) with various kinds such as zigzag, armchair and chiral GNRs in 1D. These ribbons include hydrogen atoms (hydrogens are crucial for the calculations) at the edges, which

is more realistic, to saturate the dangling bonds of carbons. The third chapter explores the electronic structure of graphene nano-ribbons with finite length and width for all types of ribbons (0D). This time, Hydrogens are added to both width and length of the ribbon. In both chapter two and three various widths are explored. Finally, the fourth chapter concludes the thesis.

Chapter 2

Graphene Nano-Ribbons in 1D

2.1 Geometry of Graphene Nano-ribbons in 1D

Graphene nano-ribbons are graphene sheets with finite size. In this section, we will describe the ribbons of 1D which is infinitely long in one of the dimensions, while the width is finite along the other direction. For generating a ribbon of 1D, we have to cut 2D graphene sheet such that one side is infinitely long (uncut), which we will define as length (L) and the other side is finite (cut in nano-scale), which will be called as width (w) to have an infinitely long rectangular shaped structure. The geometry of graphene nano-ribbons can be described with two positive integers (n,m) ($n > m$ defines all) just like defining a nanotube. These numbers show the chirality of the ribbon. If we define the lattice shown in figure 1.2, and put the coordinate system such that atom A sits at the origin and at the lattice point, $\vec{C} = n\vec{a_1} + m\vec{a_2}$ brings us to another A type atom, so another lattice point. If we cut the graphene sheet perpendicular to the line joining these two A type atoms (including half of both atoms), we have the lengths of the rectangle. The width is the equal to $|\vec{C}|$. In figure 2.1 a zigzag type graphene nano-ribbon is shown at the top and an armchair type is shown at the bottom side. To generate an armchair graphene nano-ribbon (AGNR), we have $n = c$, c being any positive integer and $m = 0$. To generate zigzag graphene nano-ribbon (ZGNR) we have

$n = m = c$. For any other combination of n and m ($n > m$), we will have a chiral graphene nano-ribbon (CGNR). The names zigzag and armchair comes from the shape of the length side of the ribbon. In figure 2.1, the length can be defined

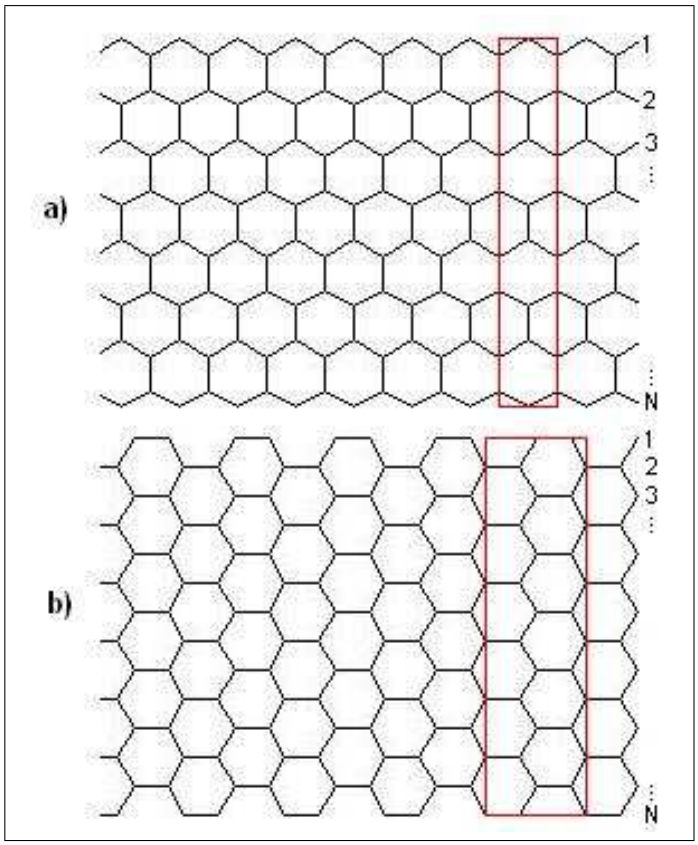

Figure 2.1: a) A zigzag graphene nano-ribbon ($N = 8$) and b) an armchair graphene nano-ribbon ($N = 14$). Red rectangles are illustrations of the unit cells used in calculations.

from left to right and the width can be defined from bottom to the top of the ribbon. In ZGNR, it can be seen that the length side has a zigzag arrangement of carbon atoms, and in AGNR, the carbon atoms make an armchair shape. In CGNR there is no specific type of arrangement. The numbers 1,2,3,...N at the right hand side of each ribbon in figure 2.1 is a definition of the width of the ribbon. If one talks about 10ZGNR, it means that in the top picture of figure 2.1, $N = 10$, so we have 10 carbon atoms along the width. The same is also true for AGNR.

In the calculation of the band structure of 1D ribbons, we take a unit cell (black rectangles in figure 2.1). Since the ribbon is infinitely long, the cell is repeated infinitely both in the right and left hand side of the rectangles. Therefore, all carbon atoms except for the ones in the first and N'th rows have three carbon atoms around. The ones at the edges (at the first and N'th row), have two carbon atoms nearby and the third sp^2 bond does not occur creating a dangling bond and making the calculation of the electronic structure difficult and misleading. Therefore, for the saturation of the dangling bonds we had to add some atoms or molecules. The easiest and mostly used atom was hydrogen [10,11,12,13,14] , so we added hydrogen atoms instead of the third carbon atom at the edges. We took the distance between carbon atom and the hydrogen atom that bounded to it to be 1.09 Å. In the calculation of 1D CGNR, we again need a unit cell that repeats itself infinitely long. In order to find how the unit cell can be formed, we have a simple operation. This operation requires the definition of chirality, the numbers n and m. The vector $\vec{C}$ joins one lattice point to another. To have a unit cell we need another vector that starts from the same lattice point as $\vec{C}$, goes perpendicular to it and ends up in another lattice point. Such a vector can be defined as $\vec{T} = p\vec{a_1} + q\vec{a_2}$, where p and q are integers that will be defined with the help of n and m. To find p and q we define a number d which is the greatest common divisor of 2n+m and 2m+n. Now that we defined d, we can have p and q as follows [15];

$$p = \frac{2m+n}{d} \tag{2.1}$$

$$q = -\frac{2n+m}{d}. \tag{2.2}$$

Figure 2.2 shows the unit cell of a 1D CGNR where $n = 4$ and $m = 1$. Here, greatest common divisor of $2n + m = 9$ and $2m + n = 6$ is $d = 3$. Therefore, $p = 6/3 = 2$ and $q = -9/3 = 3$. So $\vec{T} = 2\vec{a_1} - 3\vec{a_2}$. With the reputation of unit cell along $\vec{T}$ infinitely many times, we have 1D 4-1 CGNR.

For the tight binding calculation, we need some more parameters as we added hydrogen atoms in the system. These parameters should include hydrogen-carbon interaction and hydrogen self energy. We do not need hydrogen-hydrogen interaction since they will be too far away from each other to have a noticeable

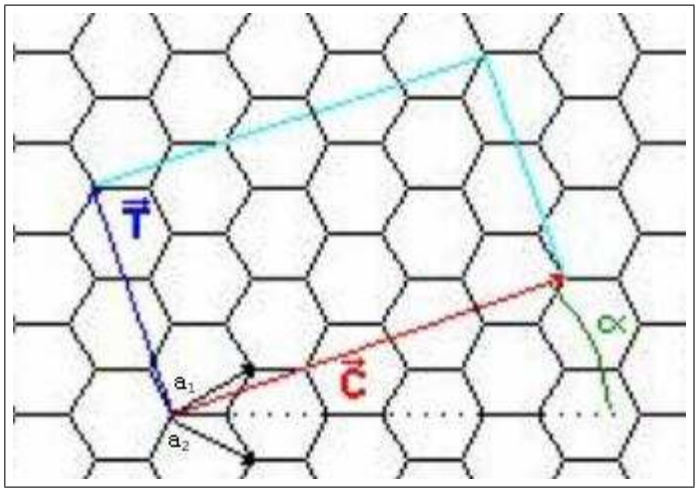

Figure 2.2: A Chiral Graphene Nano-Ribbon. a_1 and a_2 are unit vectors, red line shows $\vec{C} = 4\vec{a_1} + 1\vec{a_2}$, and dark blue line represents $\vec{T} = 2\vec{a_1} - 3\vec{a_2}$, these two lines with light blue ones enclose the unit cell of 4-1 CGNR. α is the chiral angle.

contribution. Also, these new parameters should be consistent with the ones we use for carbon atoms. We need three new parameters showing hydrogen self energy, the interaction between s orbital of hydrogen and s orbital of carbon and the interaction between s orbital of hydrogen and p orbital of carbon. To calculate these parameters we made a fitting program for three molecules CH, CH_4 and C_2H_4 all of which include only hydrogens and carbons [16,17,18,19,20]. This fitting program generated the necessary three parameters including the ones shown in table 1.1. These new parameters are; $\epsilon_H = 6.85eV$, $H_{Hs-Cs} = 7.66eV$, $H_{Hs-Cp} = -9.92eV$ for a distance of $1.09\mathring{A}$ between hydrogen and carbon atoms. The generated band structures of hydrogen added graphene nano-ribbons have a good agreement with the ones in the literature. Band structures of 1D GNRs is discussed in the following sections.

2.2 Electronic Structure of 1D ZGNR

For ZGNR, the length side has zigzag shape and the width side has armchair shape. The hydrogens are added to the first and N'th row carbon atoms as

shown in figure 2.3.

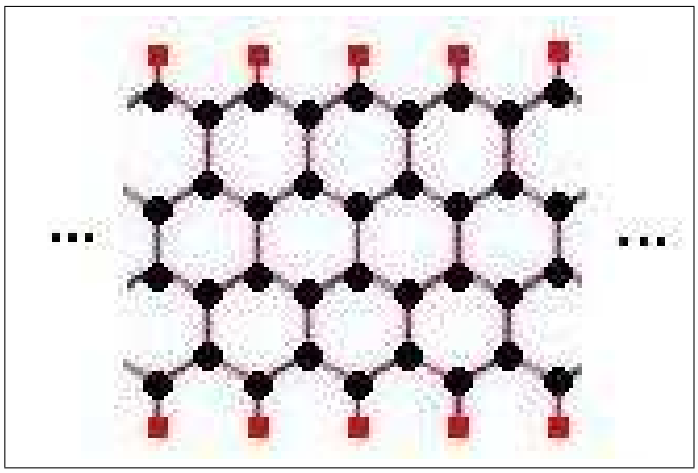

Figure 2.3: A hydrogenated zigzag graphene nano-ribbon. Red dots represents the hydrogen atoms.

In this work we calculated the band structure of 1D ZGNRs up to N=150. There is not much work in the literature with such a huge width up to now. At this width, the calculation includes 302 atoms, two of which are hydrogen atoms. To calculate the band structure of such a ribbon we have to find the eigenvalues of the hamiltonian matrix (see Section 1.3) of size (1202x1202) at each $\vec{k}$ point. Figure 2.4 [10] shows a comparison of calculated band structure 1D 10ZGNR with the one in the literature. Although everything related to the calculation of the bands is different, the similarities in band structure are obvious. Red lines represent the valance bands, whereas blue ones stand for conduction bands. Valance and conduction bands touch each other after K point and the two states become degenerate up to M point. Other conduction bands become degenerate at M point just like the valance bands. At Γ point we have a band gap around 7 eV in both graphs. Also some bands, marked with green dots, does not obey the general trend. Some of these bands in conduction band could not be observed, however, in valance band we have more or less the same behaviour of the bands.

In figure 2.5, band structures of various ZGNRs in 1D is shown. 30ZGNR has a width of 6.32 nm and 150ZGNR has 31.9 nm as a width. The easiest to recognize,

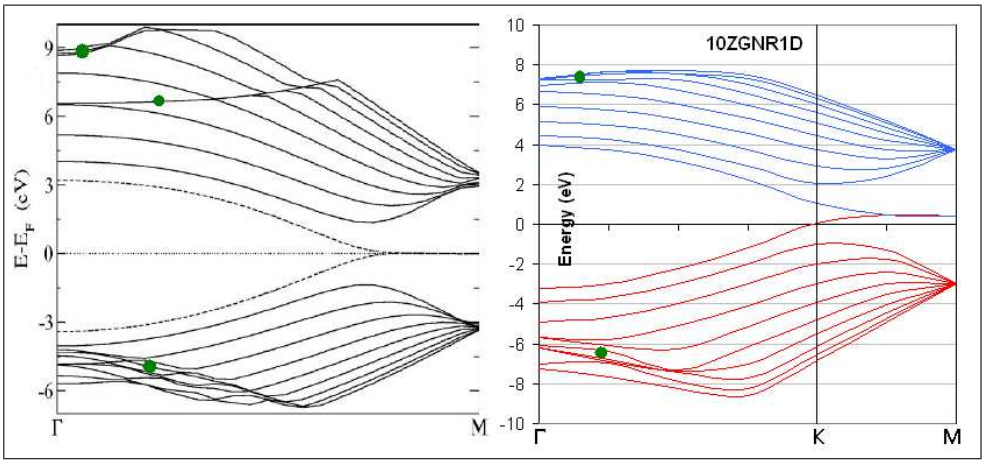

Figure 2.4: A comparison of calculated band structure of 1D 10ZGNR (on the right) with the one in the literature. $\vec{k}$ points are chosen to start from Γ and ends up at M passing over K. Red lines represent valance and blue ones represent the conduction bands. (Reproduced from L. Pisani, J. A. Chan, B. Montanari, and N. M. Harrison, Phys. Rev. B **75**, 064418 (2007).)

all of them show metallic behaviour since valance and conduction bands cross each other after K point resulting in zero band gap. Also the bands gets denser as the width increases. This is an expected result, since as the width approaches to infinity, there should stay only 8 different states as in 2D graphene. Another result that can be depicted from the graphs is that, valance and conduction bands tend to separate after they touch each other. The highest valance band and the lowest conduction band is no more degenerate when we go to greater widths. If we look at (f) in figure 2.5, we can see it immediately. This result is also understandable since at limit, the bands touch each other at K point and no where else (in 2D graphene).

Conclusion for 1D ZGNRs is that they are always metallic, and it is easy to recognize that the bands get denser since we approach to 2D graphene as we increase the width.

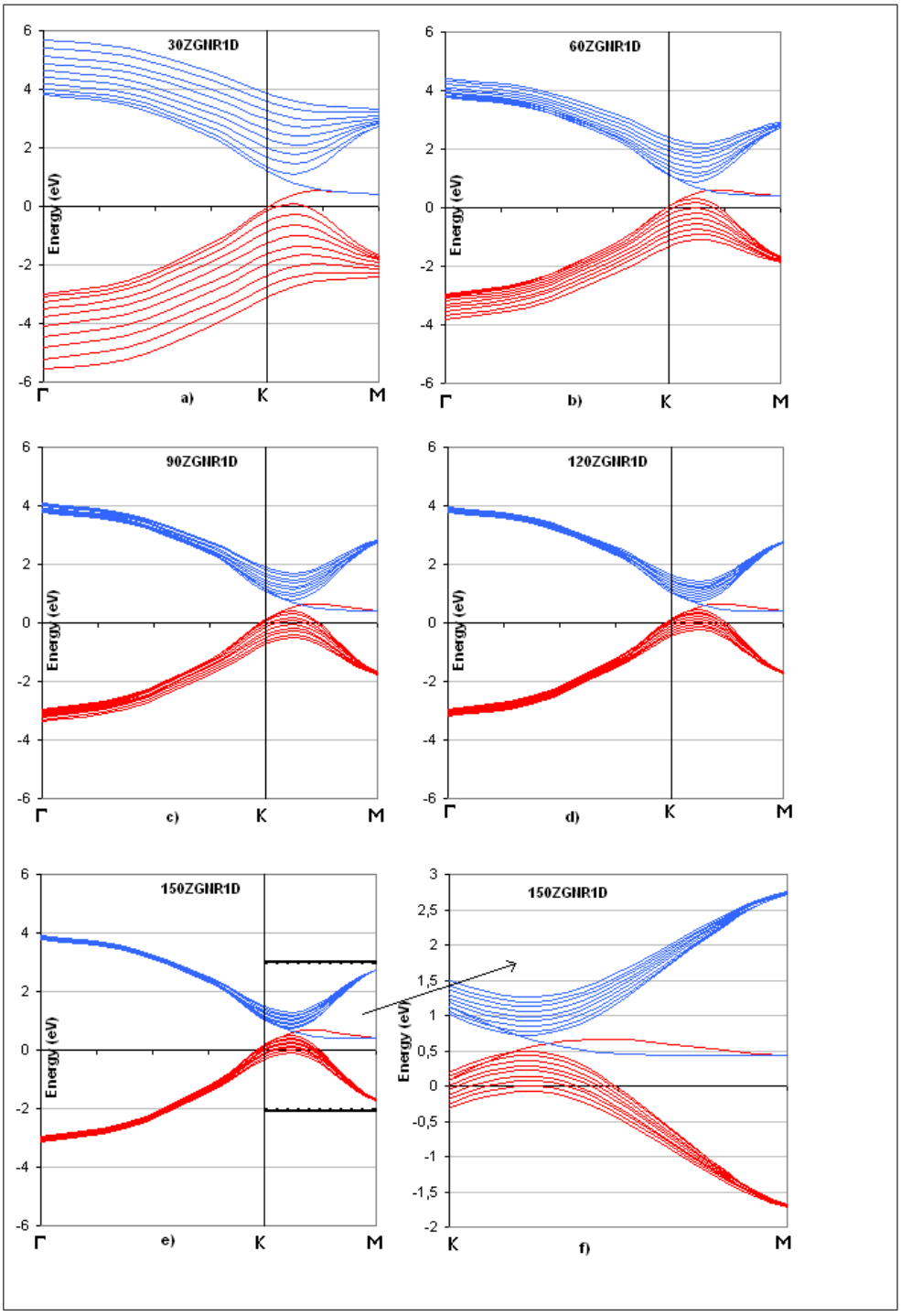

Figure 2.5: Calculated band structures starting from 30ZGNR up to 150 ZGNR in 1D. a) Band structure of 30ZGNR b) Band structure of 60ZGNR c) Band structure of 90ZGNR d) Band structure of 120ZGNR e) Band structure of 150ZGNR f) A zoomed piece of (e) showing the portion between K and M points.

2.3 Electronic Structure of 1D AGNR

For AGNR, the length side has armchair shape and the width side has zigzag shape. The hydrogens are added to the first and N'th row carbon atoms as shown in figure 2.6.

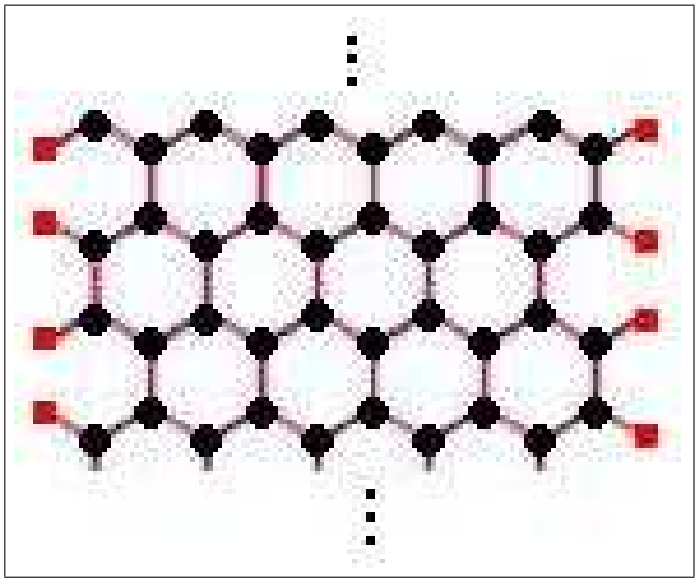

Figure 2.6: A hydrogenated armchair graphene nano-ribbon. Red dots represents the hydrogen atoms.

In this work we calculated the band structures of 1D AGNRs up to $N = 151$. At such a huge width for a graphene nano-ribbon (GNR), we have 306 atoms in the unit cell 4 of which are hydrogen atoms. Figure 2.7 shows a comparison of the bands structures that we calculated with the ones in the literature [11] for 12AGNR, 13AGNR and 14AGNR. There are 3 different groups to compare. The reason for three different groups will be explained later. Looking at figure 2.7 (a), and compare it with (b), we can say that band structures are pretty similar to each other. Band gaps are around 0.7eV around Γ point in both graphs. The behaviour of bands are almost the same, and also the crossings of the bands shown as green dots occur more or less in the same way. When we compare 13AGNRs, although band gap is around 0.8eV in both graphs (c) and (d), and the bands

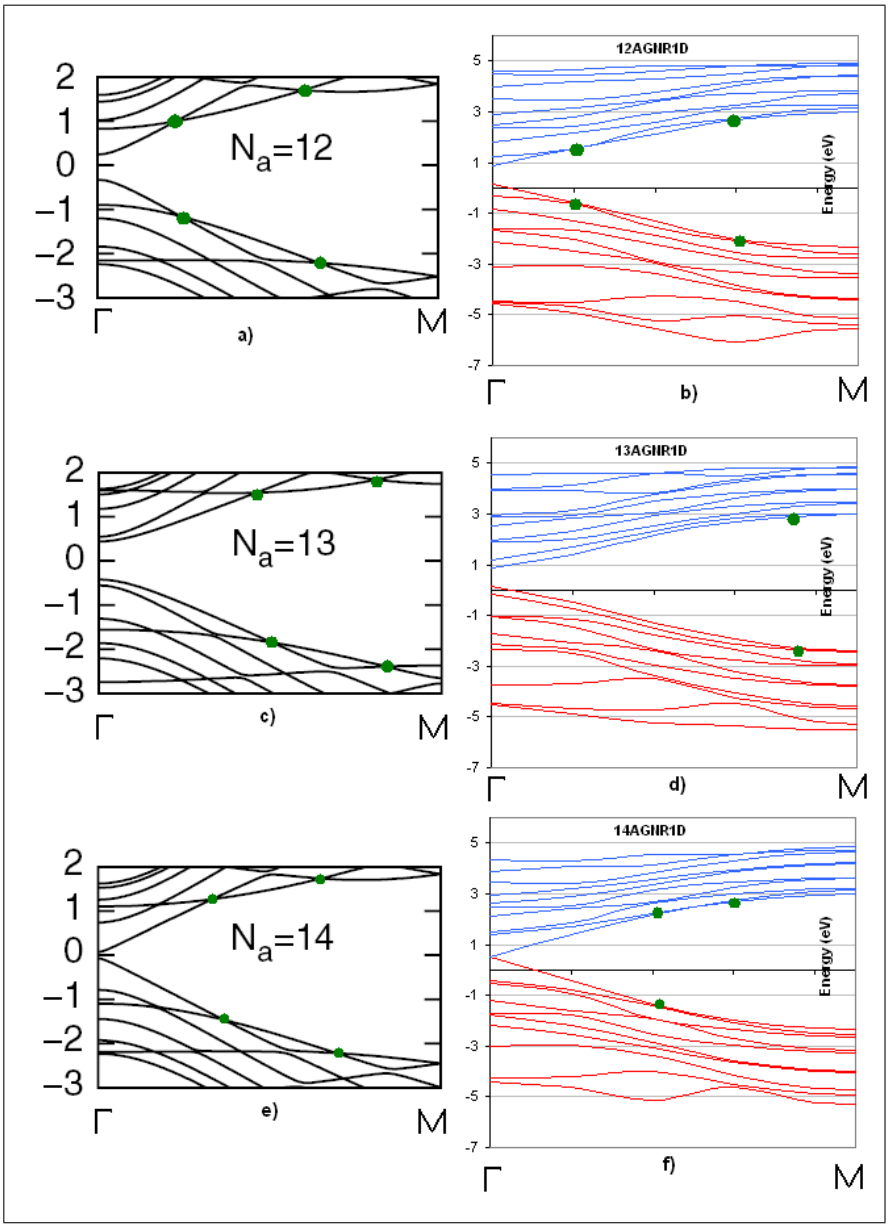

Figure 2.7: Band structures of $N = 12$,13 and 14 AGNRs. Band structures of a)$N = 12$, c)$N = 13$, e)$N = 14$ AGNRs from the literature. Calculated band structures of b)$N = 12$, d)$N = 13$, f)$N = 14$ AGNRs. (Reproduced and adapted from [Young-Woo Son, et.al. PRL 97, 216803 (2006)])

behave the same way, there is a problem with some of the crossings of the bands shown as green dots. But the general structure is generated. When we come to $N = 14$ AGNRs, we see that the structure is almost perfectly generated except for one of the green dots. At (e) it seems there is a tiny band gap, however, band gap should be zero in a tight binding calculation as the author of the same paper suggests in figure 2.8 [11].

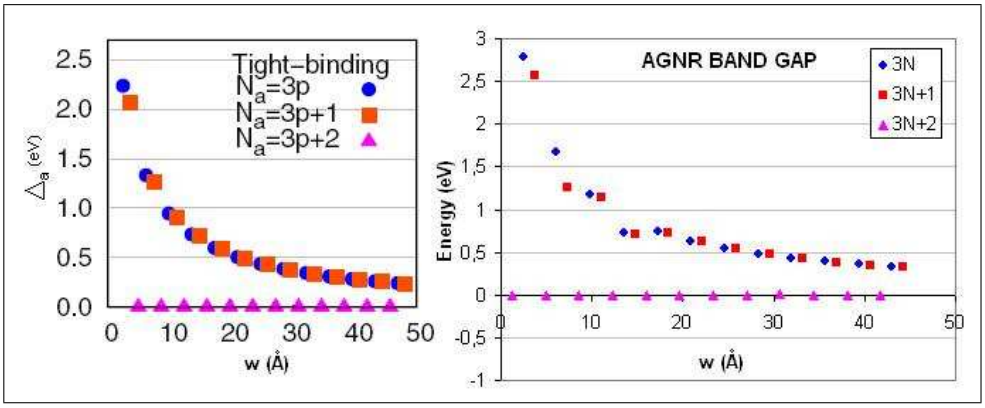

Figure 2.8: Comparison of band gap of 1D AGNRs versus width calculated, with the one in the literature. There are 3 main groups, $3N$, $3N+1$ and $3N+2$ shown as blue dots, red squares and pink triangles respectively. (Adapted from Y.-W Son, M. L. Cohen, and S. G. Louie, Phys. Rev. Lett. **97**, 216803 (2006).)

Figure 2.8 shows three groups for the width two of which behave the same way. If we have pAGNR and p is equal to $3N$ or $3N + 1$, N being an integer; we have an AGNR with a band gap. Since $12 = 3 * 4$ and $13 = 3 * 4 + 1$ ($p = 4$), we have a ribbon with a band gap as indicated in figure 2.7 (b) and (d). However, since $14 = 3 * 4 + 2$, we have zero band gap in figure 2.7 (f). The two graphs in figure 2.8 are in pretty good agreement. For AGNRs with a band gap, when the width is greater than 10 Å, the band gap decreases below 1eV. When the width reaches to 25 Å, the band gap decreases to 0.5eV. When the width becomes 40 Å, the band gap is around 0.3eV in both graphs. The main idea of the figures is that 1D AGNRs have zero band gap if we have a width such that $p = 3N + 2$, and have a finite band gap if $p \neq 3N + 2$ [11,21]. Another result that can be depicted from the figures is that the band gap decreases as the width increases.

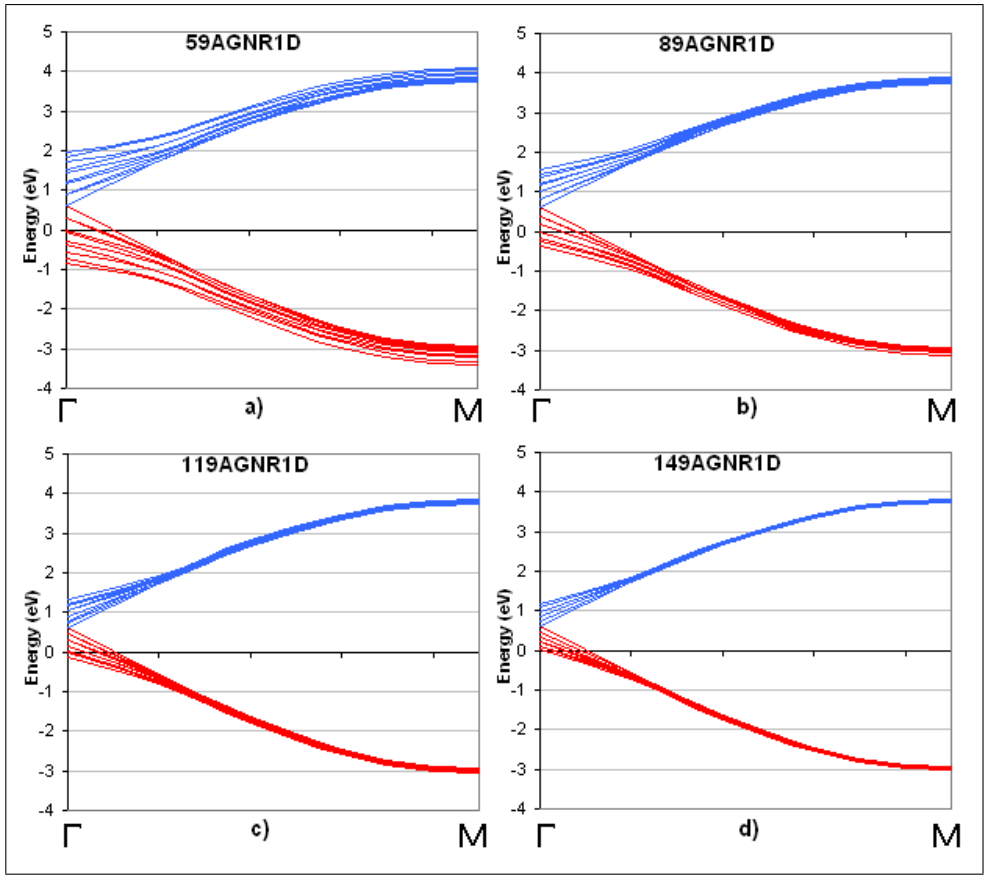

Figure 2.9: Band structure of 1D AGNRs with various widths. All of them have a width of type $3N + 2$.

What happens if we have much greater 1D AGNRs? Figure 2.9 show greater 1D AGNRs of type $3N + 2$. As it can be seen all of them have zero band gap.

They all obey the $3N + 2$ type behaviour. Also, the bands tend to get denser as the width increases. This is an expected result since at limit, we will end up with 8 different bands as in 2D graphene. However, in 2D graphene valance and conduction bands does not touch at Γ point. Instead, they become degenerate at K point as shown in figure 1.6. Therefore, somehow, at limit the valance and conduction bands have to separate at Γ point to satisfy the condition for 2D graphene. Since our periodicity is in one direction, we cannot see this effect whatever the width is.

Figure 2.10 shows the band structures of $3N$AGNRs (on the left) and $3N +$ 1AGNRs (on the right) as a function of width. All of the band structures (a-h) have a band gap which decreases as the width increases. Also, as the width gets larger, the bands become denser just like the previous band structures did. In fact, there is no satisfactory reason to make a distinction between $3N$AGNRs and $3N+1$AGNRs. Therefore, we have two distinct groups as $3N+2$AGNRs and the remaining ones, for 1D AGNRs. It will be clearer if we look at figure 2.11 that we cannot separate $3N$ type and $3N + 1$ type AGNRs. In this figure, almost all of the red squares are on top of blue dots showing the same band gap for $3N$ and $3N + 1$ AGNRs.

In figure 2.11 the width starts from 50AGNR (60.26 Å) and goes up to 151AGNR (184.5 Å). These AGNRs are much more greater than we presented previously. It is not so easy to obtain even 2D graphene experimentally. Therefore, it will be too difficult to cut it as small as 10-20AGNR (around 20 Å). That's why 50-150AGNRs are much more realistic and important than smaller ones for now. Although they are important, they have a band gap smaller than 0.25eV decreasing their capability to be used as semiconductor devices for applications. After $w > 100$ Å, we have a band gap less than 0.15eV and even smaller than 0.1eV for $w > 150$ Å. It gets smaller and smaller as the width gets larger.

In conclusion, 1D AGNRs can be classified in two different groups. One of the groups is $3N + 2$ group in which all ribbons are semi-metal having zero band

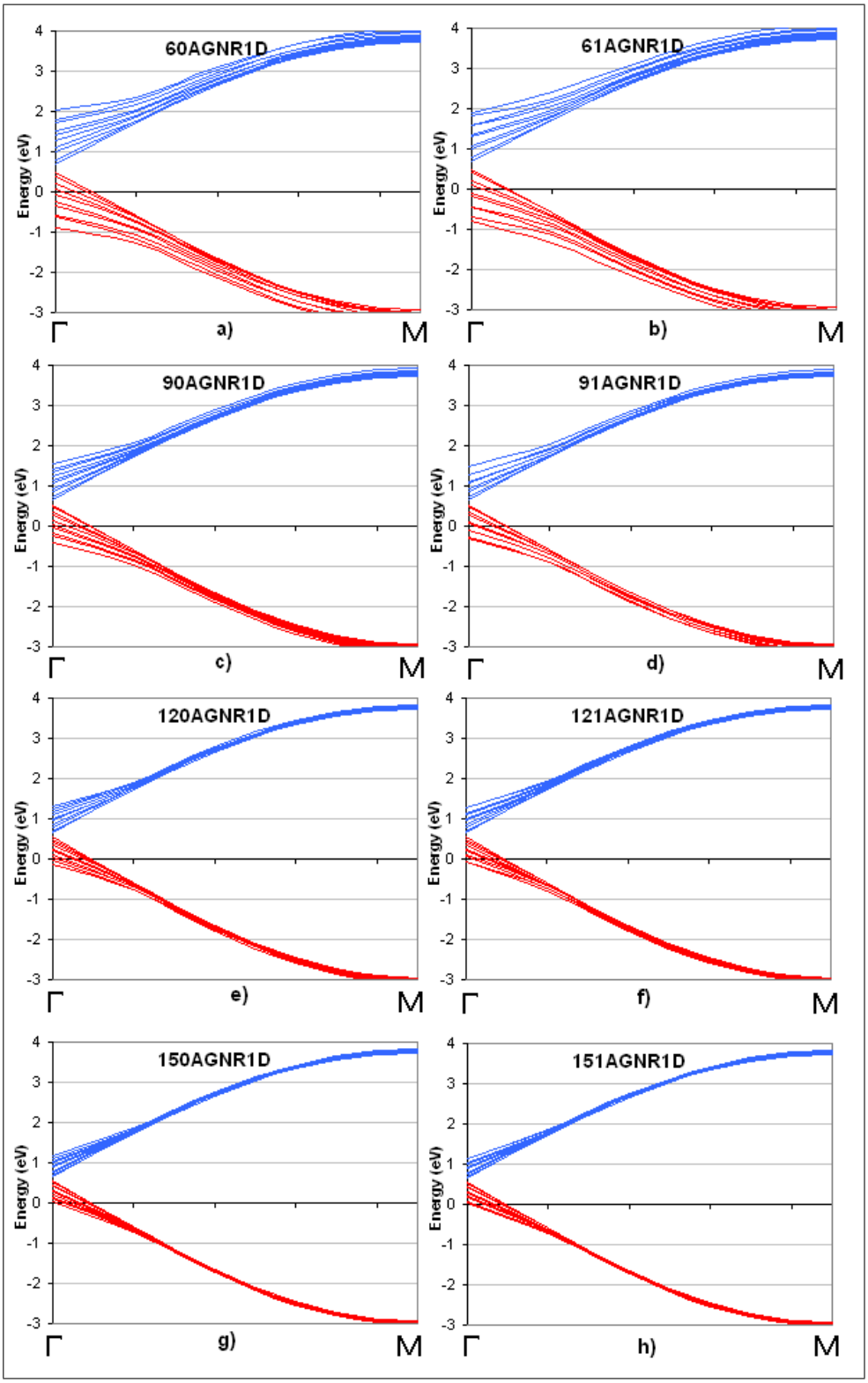

Figure 2.10: Band structure of 1D AGNRs with various widths. Graphs on the left hand side have a width of type $3N$, and graphs on the right hand side have a width of type $3N + 1$.

gap since valance and conduction bands touch each other at Γ point. The second

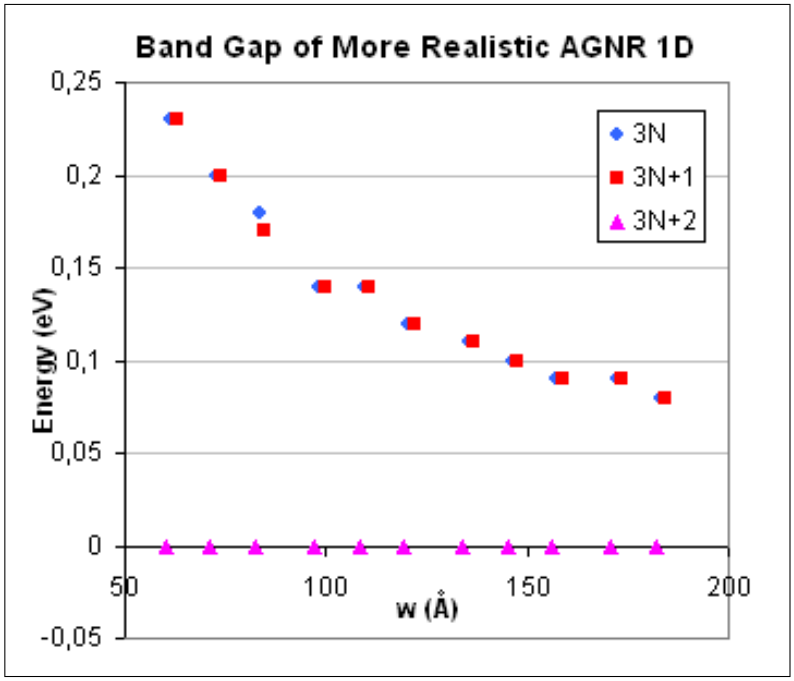

Figure 2.11: Band gaps of 1D AGNRs of three types as a function of width. $3N$, $3N+1$ and $3N+2$ shown as blue dots, red squares and pink triangles respectively.

group is the rest of AGNRs ($3N$ and $3N+1$) in which all ribbons have a finite band gap showing semiconducting behaviour. The band gaps of this second group members tend to decrease as the width increases. Calculations show that they get below 0.1eV as the width gets above 150 Å.

2.4 Electronic Structure of 1D CGNR

CGNRs are graphene nano-ribbons that do not have an edge in zigzag or armchair shape. In fact they can have various shapes depending on the chirality. CGNRs can be defined with two positive integers n and m ($n > m$). When m equal to n we have a ZGNR in which vector $\vec{C} = n\vec{a_1} + m\vec{a_2}$ is parallel to x axis, and when m equal to zero we have an AGNR in which vector $\vec{C}$ makes an angle of $\frac{\pi}{6}$ with

x axis. Therefore, in all CGNRs, $\vec{C}$ makes an angle $0 < \alpha < \pi/6$ with the x axis as shown in figure 2.2. The region $\pi/6 < \alpha < \pi/3$ is the reputation of the same CGNRs in reverse order (from ZGNR to AGNR).

CGNRs are important because there is no work about them in the literature. Calculations related to CGNRs will be one of the most important contributions that we will make to the literature. Figure 2.12 shows the unit cell of 10-1CGNR. Since $n = 10$ and $m = 1$, d, p and q can be calculated as $d = 3$, $p = 4$ and $q = -7$ by using equations 2.1 and 2.2. This can also be checked by looking at the figure. Vector $\vec{C}$ makes an angle with x axis $\alpha = 25.28^o$. Since we have 148

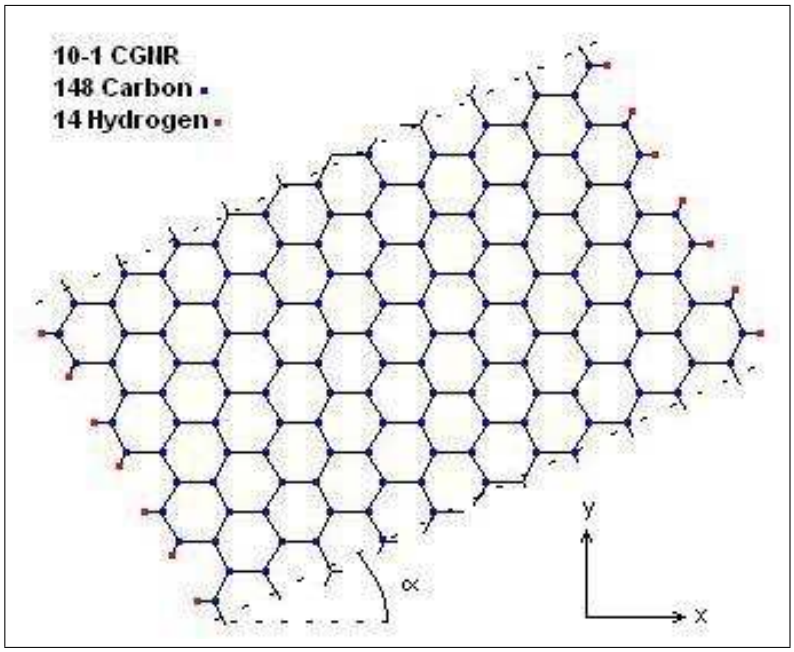

Figure 2.12: Unit cell of 1D 10-1CGNR is shown. Blue dots represents 148 Carbon atoms, and red dots represents 14 Hydrogen atoms. The unit cell repeats itself along non-hydrogenated carbon atoms.

carbon and 14 hydrogen atoms inside the unit cell, the calculation includes 162 atoms, which is not the greatest one that we calculated. The smallest CGNR is 4-1 CGNR (shown in figure 2.2) which has 28 carbon and 6 hydrogen atoms in its unit cell.

If we think of the angle although 10-1CGNR is close to be an AGNR, it has

a very different band structure. Figure 2.14 shows the band structure of 1D 10-1CGNR. It is quite different from any figure of AGNRs such as the ones in figure 2.10. Valance and conduction bands are farthest at Γ point and closest at $\vec{k} = \frac{\pi}{|\vec{T}|}$ opposing to the band structure of AGNRs. In fact, the structure much more looks like the band structure of ZGNRs. However, for 10-1CGNR, there is a band gap of 0.3eV, which does not occur in a ZGNR. Therefore, the angle α seem not to have a major effect on the band structure. May be, it can have an effect on the value of band gap. Figure 2.13 (a) shows how band gap of 1D CGNRs change with angle α. There are oscillations in the value of band gap as the angle changes from zero to 30^o. However, there is no straight forward dependence.

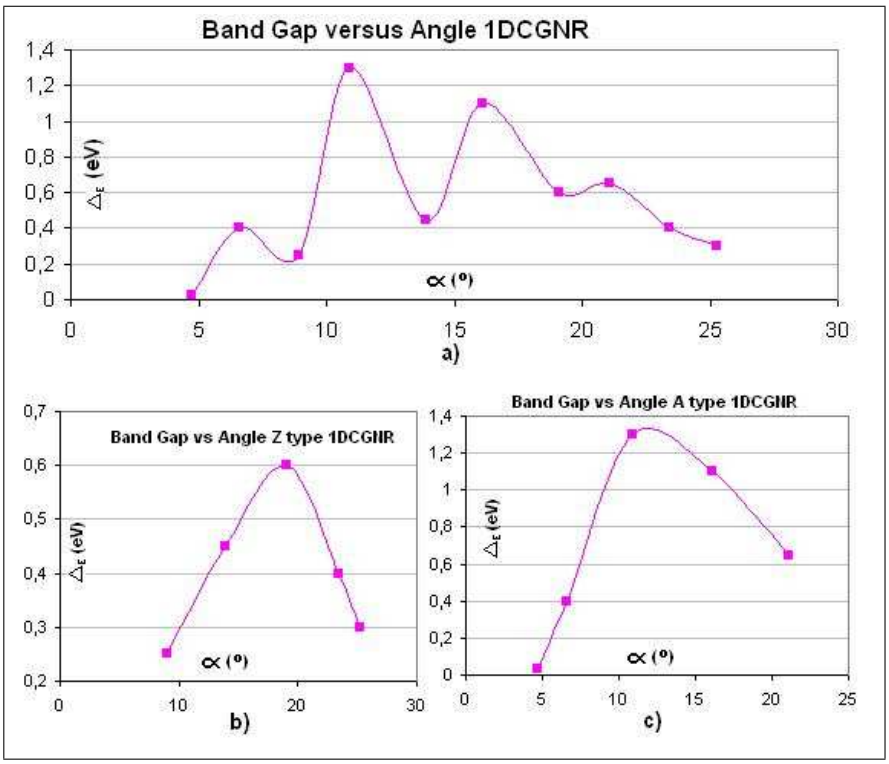

Figure 2.13: (a) Band gap versus Angle 1DCGNR for all CGNRs. (b) Band gap versus Angle for ZGNR type 1DCGNRs. (c) Band gap versus Angle for AGNR type 1DCGNRs.

There are two types of different band structures for CGNRs. One of them can be called ZGNR type just like the band structure of 10-1CGNR and AGNR type

which we will deal later. The CGNRs shown in figure 2.15 are the ones that are ZGNR type. In the figure, 4-1CGNR, 7-4CGNR, 5-2CGNR and 7-1CGNR are shown in (a),(b),(c) and (d) respectively. They have similar band structures but also they have different band gaps. 4-1CGNR has a band gap of 0.6eV, while 5-2CGNR has the second greatest with 0.45eV among this type CGNRs. 7-1CGNR has 0.4eV, 10-1CGNR has 0.3eV and 7-4CGNR has 0.25eV of band gap.

For 4-1CGNR $\alpha = 19.1^o$, 5-2CGNR $\alpha = 13.9^o$, 7-1CGNR $\alpha = 23.4^o$, 10-1CGNR $\alpha = 25.3^o$ and 7-4CGNR $\alpha = 8.9^o$ as shown in figure 2.13 (b). The figure show it clearly that ZGNR type CGNRs can have a dependence on angle.

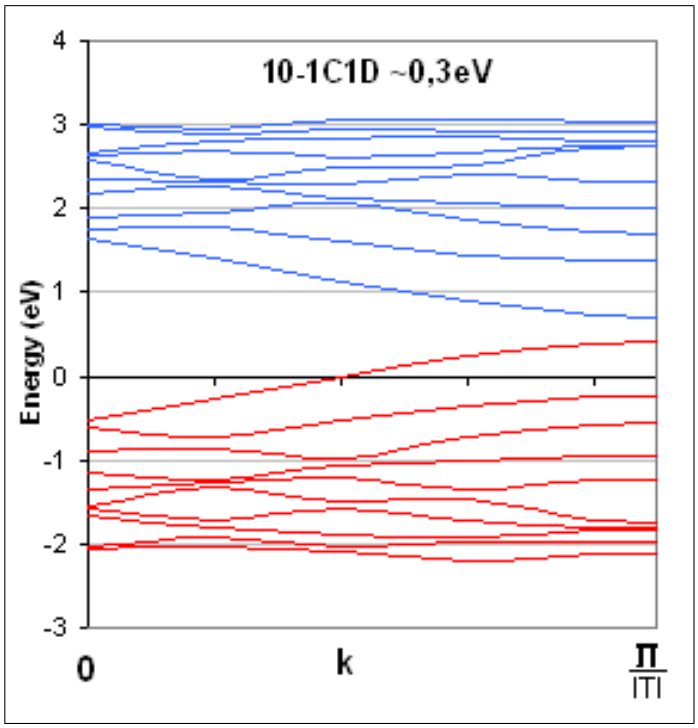

Figure 2.14: Band structure of 1D 10-1CGNR. Energy eigenvalues versus $\vec{k}$ points.

As we go from zero to 30^o, the band gap increases at first, makes a peak and then slowly decreases making a Gaussian like distribution. The sum of n and m, seems to have a proportionality with band gap. For 4-1CGNR, 5-2CGNR, 7-1CGNR, 10-1CGNR, 7-4CGNR $n + m = 5, 7, 8, 11, 11$ respectively. By looking at this result it can be depicted as the sum $n + m$ increases, the band gap decreases.

Since the length of the vector $\vec{C}$ is almost proportional to the sum of n and m, the same idea can be applied for the length of $\vec{C}$. As the length of $\vec{C}$ increases, the band gap decreases for ZGNR type CGNRs.

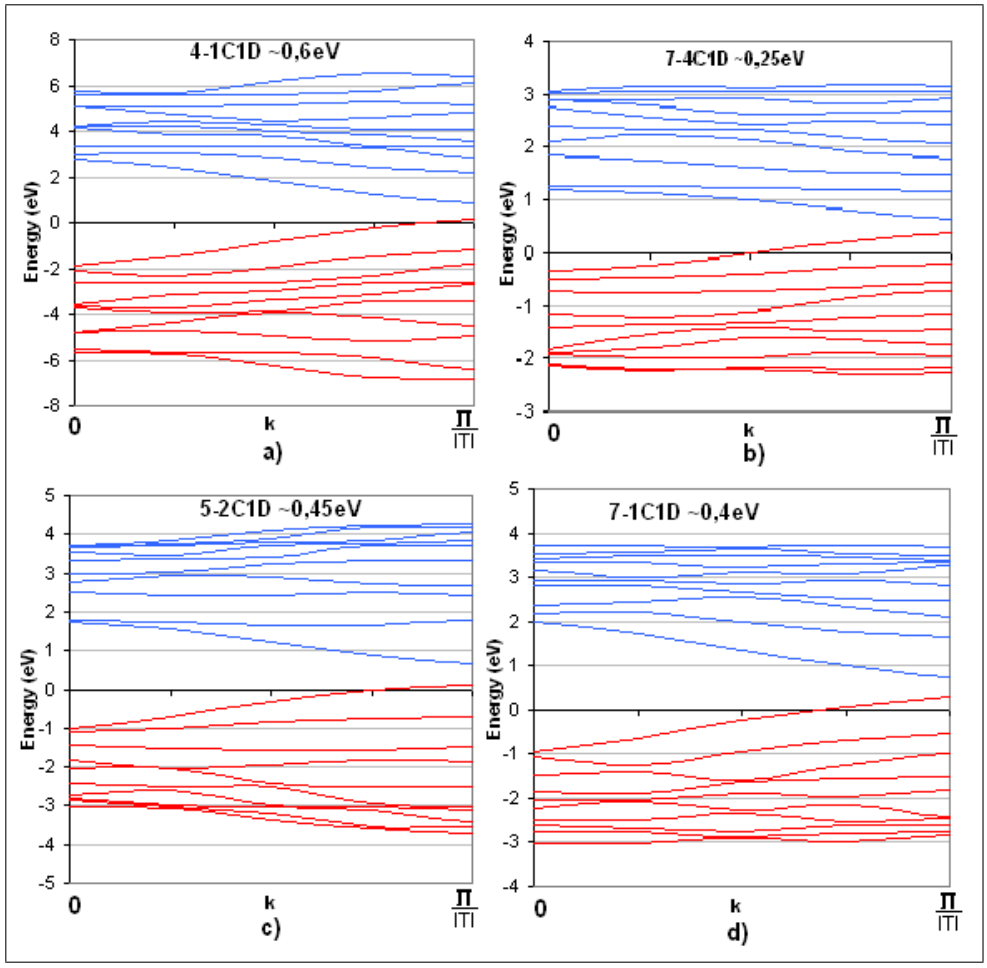

Figure 2.15: Band structures of various ZGNR type CGNRs. a)4-1CGNR, b)7-4CGNR, c)5-2CGNR, d)7-1CGNR

The second type of CGNRs were said to be AGNR type which are shown in figure 2.16. When we look at the band structures, we can recognize that they are much more like the band structure of 1D AGNRs as shown in figure 2.7. Here, as we go from (a) to (e), the band gap decreases. In figure 2.16 (a), 2-1CGNR is shown with a band gap of 1.3eV. In (b), we have 3-1CGNR with 1.1eV of band gap and in (c) 5-1CGNR with a band gap of 0.65eV. Finally in

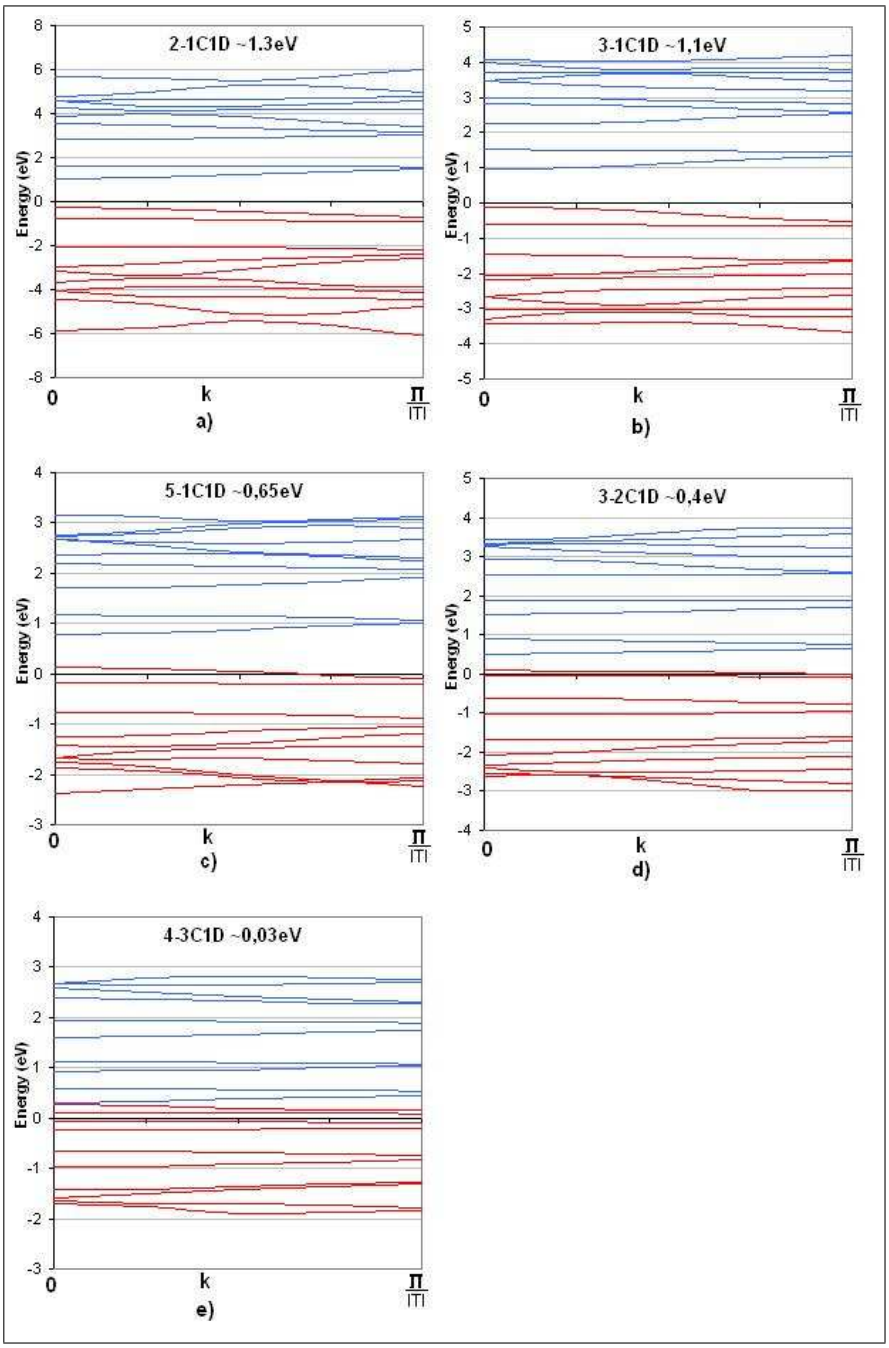

Figure 2.16: Band structures of various AGNR type CGNRs. a)2-1CGNR, b)3-1CGNR, c)5-1CGNR, d)3-2CGNR, e)4-3CGNR

(d) and (e) we have 3-2CGNR and 4-3CGNR with 0.4eV and 0.03eV of band gap respectively. Figure 2.13 (c) shows how the band gap of this type 1D CGNRs depend on angle. Again, as in ZGNR type CGNRs there seems to be a Gaussian

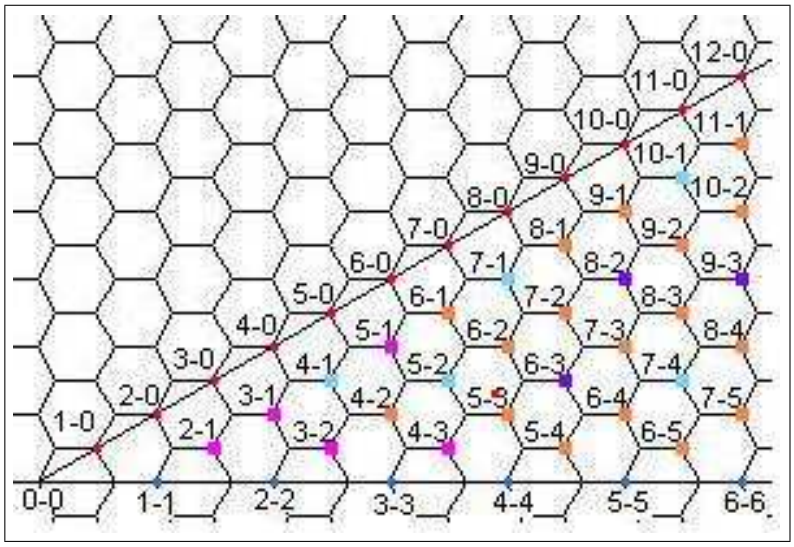

Figure 2.17: n and m values for $\vec{C}$ starting from the origin (0-0). Blue dots represent ZGNRs, red dots represent AGNRs and in between lies CGNRs. Light blue dots show ZGNR type CGNRs and pink dots show AGNR type CGNRs that are presented in this work. Purple dots stand for CGNRs that are expected to be ZGNR type and orange dots are for CGNRs to be AGNR type.

distribution. Also, the same assumption we made for ZGNR type CGNRs seem to hold here as well. As the vector $\vec{C}$ gets longer, the band gap decreases. The exception that challenges the assumption made is that 3-2CGNR have smaller a band gap than 5-1CGNR. There is one more thing to recognize while comparing figure 2.15 and 2.16. AGNR type CGNRs starts from a higher value of band gap with respect to ZGNR type, however, they decrease with the increase in $|\vec{C}|$ much faster. For 4-3CGNR $|\vec{C}| = 28.3$ Åand band gap has the value 0.03eV, whereas, for 7-4CGNR $|\vec{C}| = 44.8$ Åand it has a band gap of 0.25eV.

Figure 2.17 shows AGNRs, ZGNRs and different CGNRs with different types. Light blue dots stand for AGNR type CGNRs that are presented in this work, whereas pink dots represent the ZGNR type CGNRs. While defining a single wall carbon nanotube (SWCNT), we use the same procedure for chirality as we used

for GNR [5]. The main difference between SWCNT and GNR is that nanotubes are the rolled up version of nano-ribbons. Therefore, for SWCNT, we have the same n and m for the definition of chiral vector $\vec{C}$. There is also a simple way of determining whether SWCNT is metal or semi-conductor depending on these numbers n and m. If $n-m$ is a multiple of three, the nanotube becomes metallic, semiconducting otherwise [22,23,24]. For CGNRs, there is a similar relationship between the numbers n and m, and the type of band structure. If we inspect carefully, all ZGNR type CGNRs we had presented, have the same property for n and m that metallic SWCNTs have. In all ZGNR type CGNRs, $n-m$ is a multiple of three. However, in none of AGNR type CGNRs $n-m$ is a multiple of three. In figure 2.17 purple dots represent CGNRs that we expect to be ZGNR type. If the expectation is true, one third of all CGNRs should be ZGNR type. In the same figure, orange dots represent CGNRs that are expected to be AGNR type for the same reason explained above. Two third of all CGNRs should be AGNR type then. Another interesting similarity between SWCNTs and GNRs is about the band gap. For a nanotube with a band gap, band gap value decreases with the increase in radius. Since nanotubes are rolled up version of GNRs, the radius depends on the chiral vector $\vec{C}$ by the following equation;

$$|\vec{C}| = 2\pi R. \tag{2.3}$$

Therefore, the radius of nanotube is directly proportional to the chiral vector with a proportionality constant $(2\pi)^{-1}$. This fact lets us to state that as the chiral vector in nanotube increases, the band gap decreases. This statement is the same as the one we made for CGNRs.

In conclusion for 1D CGNRs, CGNRs can be categorized in two distinct families. One of them is ZGNR type and the other one is AGNR type CGNRs both getting its name from the band structures. The band structure of ZGNR (AGNR) type 1D CGNRs look like the band structure of ZGNRs (AGNRs). In ZGNR type CGNRs, $n-m$ is a multiple of three whereas for AGNR type CGNRs there is no such relationship. CGNRs in both types have noticeable band gaps (maximum 1.3eV) decreasing with the increase in the length of chiral vector $\vec{C}$. We also have a Gaussian distribution for the band gap as a function of angle in both types. The angle changes between 0 and 30^o.

Chapter 3

Graphene Nano-Ribbons in 0D

3.1 Geometry of Graphene Nano-Ribbons in 0D

In this section, we will describe GNRs with finite width and length. Since both sides are finite, we have to cut the graphene in both dimensions to have a rectangle differing from 1D GNRs.

This time, since we have a 0D GNR, we have to consider it as a molecule in a tight binding calculation and look for discrete energy eigenvalues at only Γ point. In order to be able to make such a calculation we consider a unit cell much greater than the size of the molecule. Then, repeating molecules have enough empty space in between in order not to have an effect on each other. One other important difference in the calculation of 0D GNRs is that we have a finite length, so we have to put hydrogens in both dimensions of the rectangle. Figure 3.1 shows a ZGNR with hydrogens on each side of the rectangle. The ribbon is called a ZGNR since the length side has a zigzag shape. For this ribbon, $L = 33.86$ Åand $w = 13.86$ Åincluding 162 carbon atoms shown as blue dots and 38 hydrogen atoms represented by red dots thereby 200 atoms in total.

Bands for 0D ZGNR, 0D AGNR and 0D CGNR are presented in the following sections.

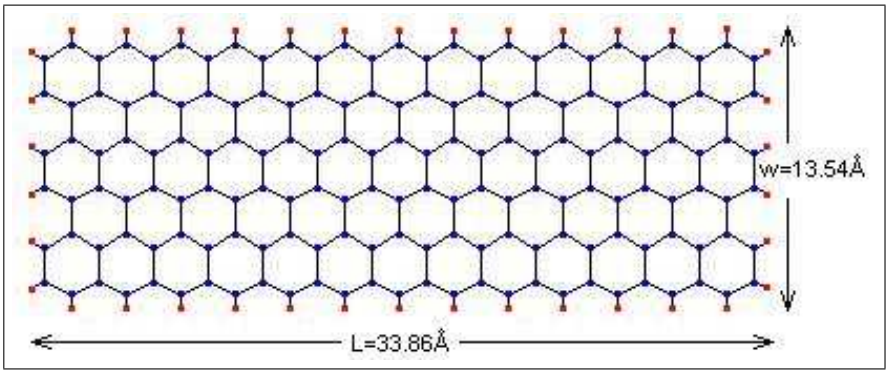

Figure 3.1: A 0D Zigzag Graphene Nano-Ribbon with $L = 33.86$ Åand $w = 13.54$ Å. Red dots represent hydrogen atoms, and blue dots stand for Carbon atoms.

3.2 Electronic Structure of 0D ZGNR

A 0D ZGNR is shown in figure 3.1. It has 27 carbon atoms joined to create zigzag edge and 6 carbon atoms to make the armchair edge. Therefore, we will call it 27Z6A-GNR in order to make the definition easier.

In this work, we present a variety of 0D ZGNRs, starting from 21Z4A-GNR as the smallest, up to 41Z10A-GNR as the greatest one. For 21Z4A-GNR, $L = 26.5$ Åand $w = 9.3$ Å, and we have 84 C, 28 H, 112 atoms in total. For 41Z10A-GNR, $L = 51.1$ Å, $w = 22.1$ Åwhich includes 410 C, 60 H, 470 atoms inside. In order to make the calculation, the Hamiltonian matrix of (1700x1700) has to be diagonalized.

Figure 3.2 shows the energy bands of a 0D ZGNR with $w = 9.3$ Åfor 26.5 Å$\leq L \leq 51.1$ Å. Blue lines corresponds to highest occupied molecular orbital (HOMO) and the red ones stand for lowest unoccupied molecular orbital (LUMO). For every width value of length in the figure, HOMO and LUMO levels touch each other. This means there is no HOMO-LUMO gap in this 0D ZGNR. In the same figure, the bands tend to get denser. This is not surprising since as the length gets larger, the molecule occupies more atoms and new energy levels. What if we change the width? Figure 3.3 show energy levels versus length of the ribbons for various widths. All of them have the same structure as figure 3.2. This shows us

that 0D ZGNRs does not have a HOMO-LUMO gap just like 1D ZGNRs don't have a band gap. Since the number of atoms in the ribbon increases as the width gets larger, the bands tend to squeeze as we go from (a) to (f).

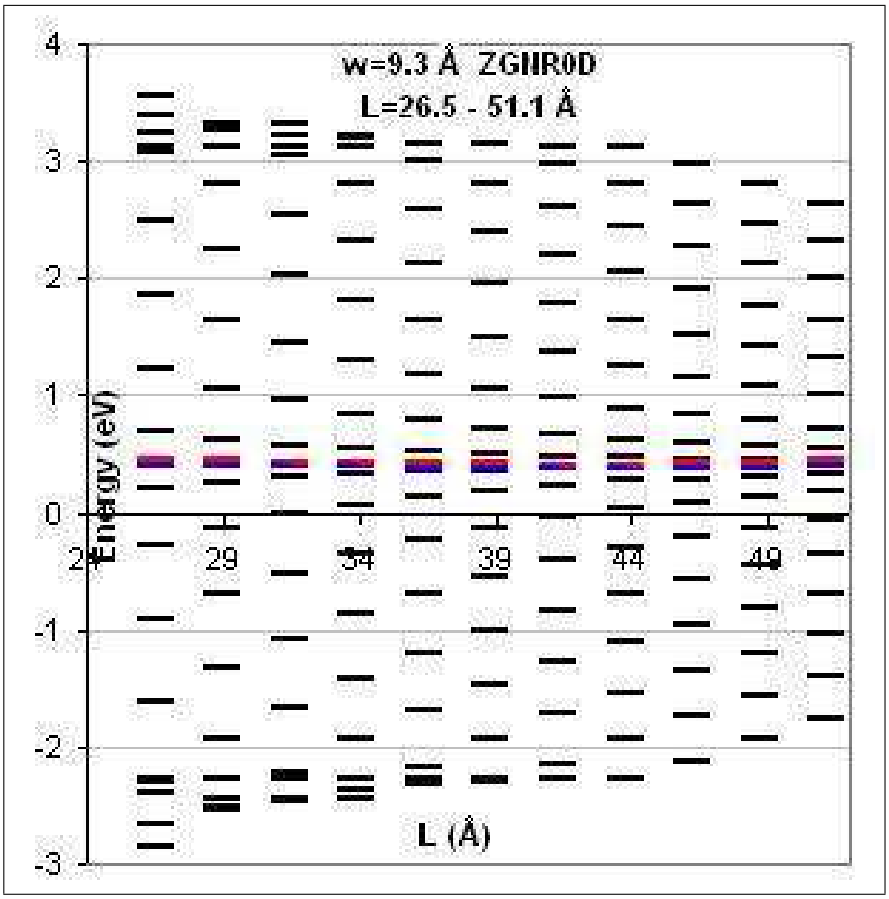

Figure 3.2: Energy levels of ZGNR with $w = 9.3$ Åfor different lengths. Red lines shown lowest unoccupied molecular orbital (LUMO) and blue lines show highest occupied molecular orbital (HOMO) levels of the molecule.

In conclusion, 0D ZGNRs does not have a HOMO-LUMO gap. The change in the length cannot open a gap as well as the change in the width. However, if we increase the size of the ribbon by increasing either its length or width, the bands tend to squeeze.

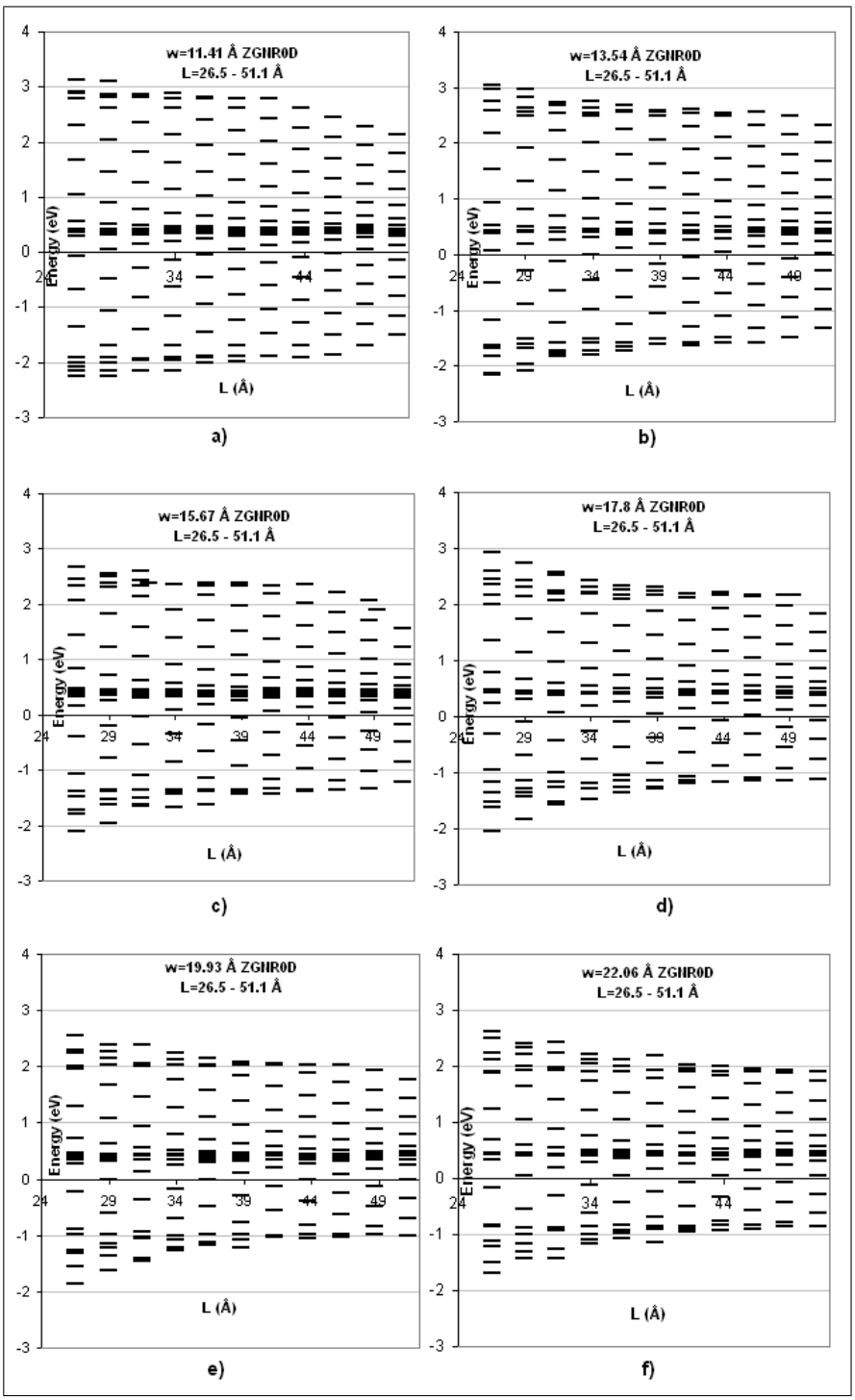

Figure 3.3: Energy levels of 0D ZGNRs. a) For $w = 11.41$ Å, b) For $w = 13.54$ Å, c) For $w = 15.67$ Å, d) For $w = 17.8$ Å, e) For $w = 19.93$ Å, f) For $w = 22.06$ Å.

3.3 Electronic Structure of 0D AGNR

A 0D AGNR has the length in an armchair and the width in zigzag shape. In this work, we present various 0D AGNRs that have different widths and lengths. 10A3Z-GNR is the smallest AGNR that we work with in which the length side has 10 carbon atoms and the width side has 3. It has 30 carbon and 22 hydrogen atoms, 52 atoms in total. The greatest AGNR we present is 30A15Z-GNR which has 450 carbon and 74 hydrogen atoms, 524 atoms in total. 10A3Z-GNR has edges of $w = 4.33$ Åand $L = 22.06$ Å, whereas 30A15Z-GNR has $w = 19.09$ Åand $L = 64.66$ Åas dimensions. In figure 3.4 energy levels of GNRs from

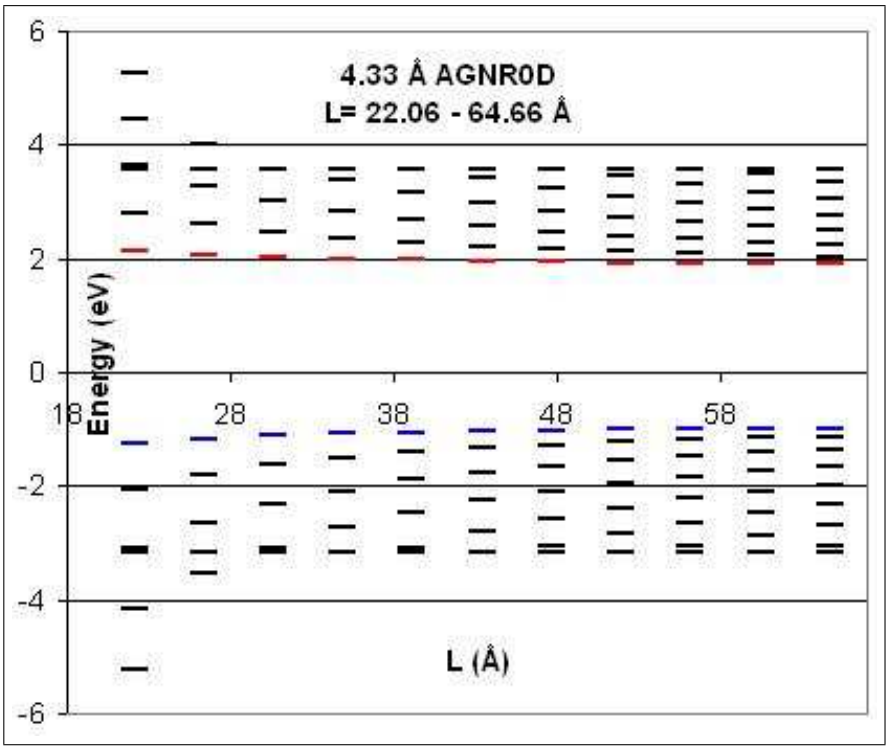

Figure 3.4: Energy levels of 0D AGNR with width 4.33 Åversus length. Blue lines represent HOMO levels and the red ones stand for LUMO levels.

10A3Z-GNR to 30A3Z-GNR is shown.

The width is the same for all energy levels as $w = 4.33$ Å, however, the length of the ribbon changes (22.06 Å$\leq L \leq$ 64.66 Å). In all cases, the ribbons have

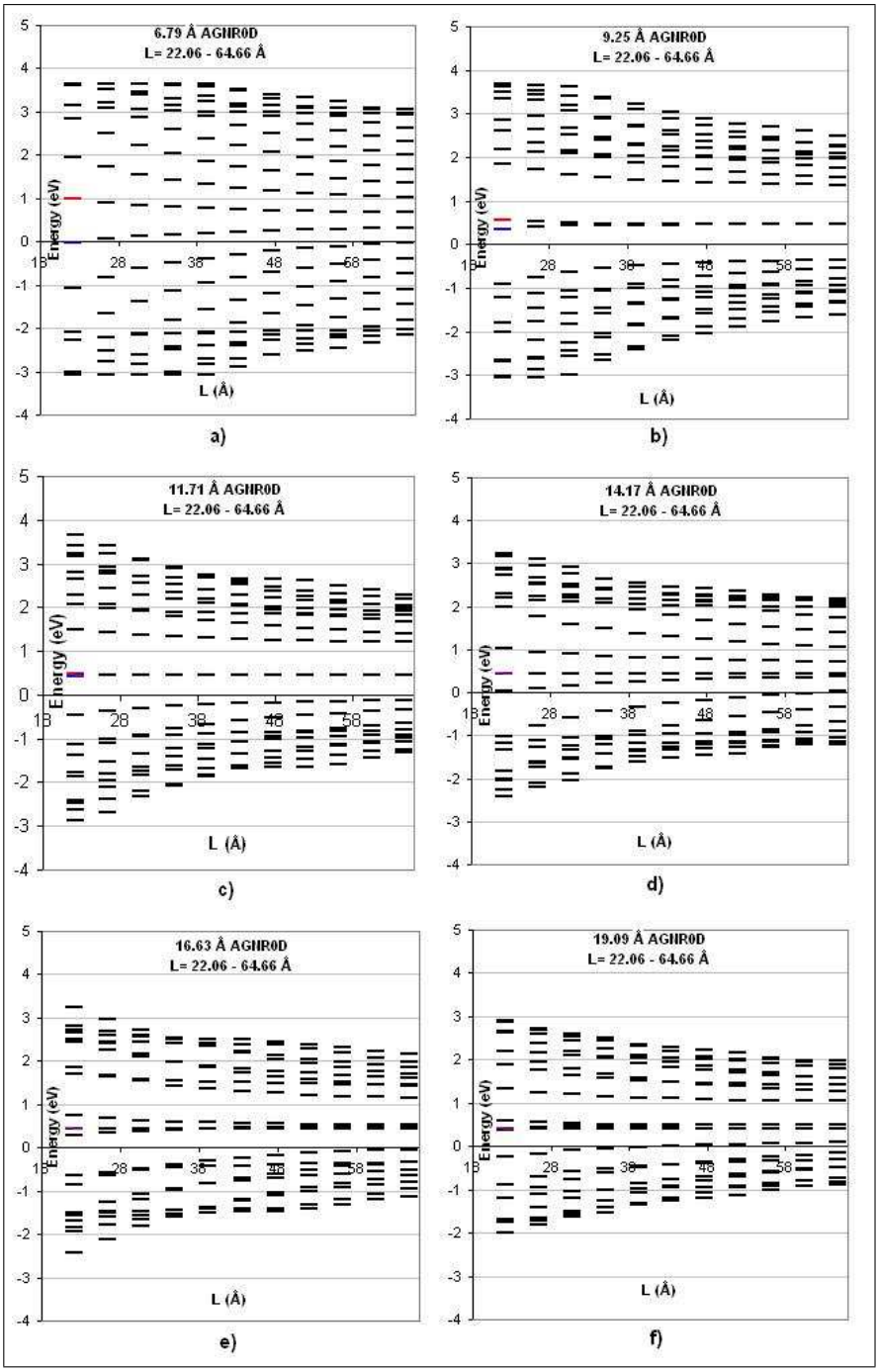

Figure 3.5: Energy levels of various 0D AGNRs. a) For $w = 6.79$ Å, b) For $w = 9.25$ Å, c) For $w = 11.71$ Å, d) For $w = 14.17$ Å, e) For $w = 16.63$ Å, f) For $w = 19.09$ Å.

a noticeable HOMO-LUMO gap. For the smallest ribbon, the value of HOMO-LUMO gap is 3.4eV. It drops slowly as the width increases and for the largest ribbon of this width we have a gap of 2.9eV.

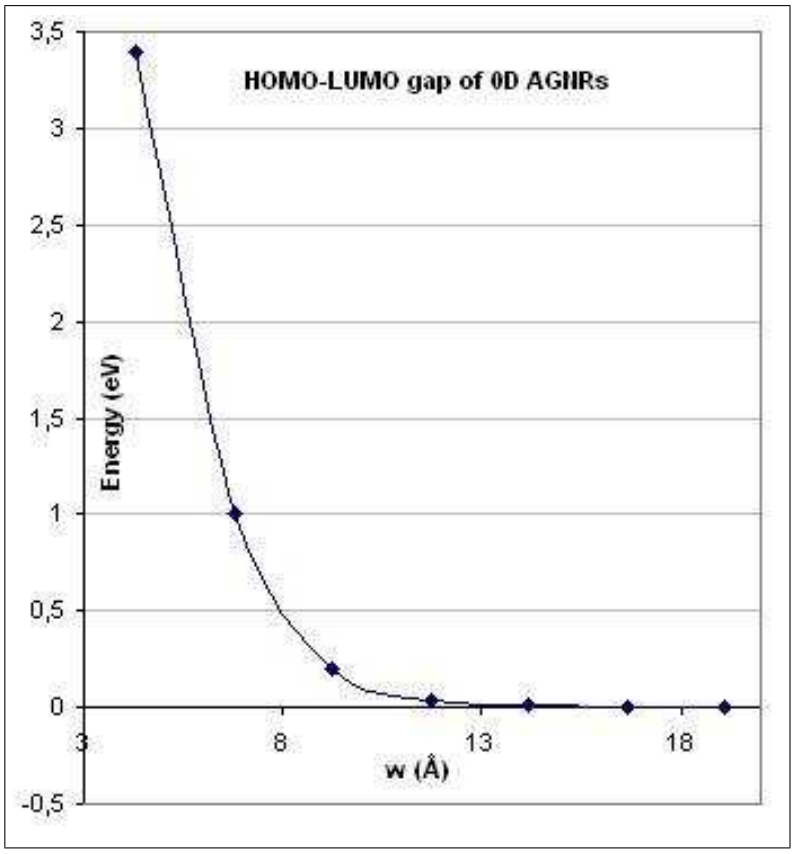

Figure 3.6: The HOMO-LUMO gap of AGNRs versus width w. $L = 22.06$ Åfor all widths.

In figure 3.5, various AGNRs are shown with different widths. They are drawn in the same length scale. The width increases as we go from (a) to (f). Notice how HOMO and LUMO levels to approach each other as we increase the width. After $w = 11.71$ Å, we do not have a gap at all. Therefore, the gap of AGNRs are both effected from the length and the width of the ribbon. As the size of the ribbon gets larger, the HOMO-LUMO gap decreases. Figure 3.6 shows how the HOMO-LUMO gap depends on width for the smallest length. It is obvious that we do not have a gap after the width gets larger than 11.71 Å. There is another

important result that can be depicted from the same graph. $3N + 2$ rule that 1D AGNRs obey do not hold here. Although $N = 5$ in figure 3.5 (a), it has a noticeable HOMO-LUMO gap and $N = 9$ for (c), which has almost zero gap.

As a conclusion, 0D AGNRs have HOMO-LUMO gaps depending on both width and length. However, after width becomes larger than 11.7 Å, we do not have a gap even for the smallest length. Therefore, the width has a greater impact on the electronic structure. Also, $3N + 2$ rule that 1D AGNRs obey does not hold in 0D AGNRs.

3.4 Electronic Structure of 0D CGNR

In this section, we present 0D chiral graphene nano-ribbons. These ribbons have great importance in this work because no one has done anything about them yet. We present 10 different 0D CGNRs as we did for 1D CGNRs. These are 2-1CGNR, 3-1CGNR, 4-1CGNR 5-1CGNR 7-1CGNR, 10-1CGNR, 3-2CGNR, 5-2CGNR, 4-3CGNR and 7-4CGNR. We have 46 atoms, 18 of which are hydrogens in the smallest CGNR (4-1CGNR), whereas 192 atoms, 42 of which are hydrogens, in the greatest one, namely 4-3CGNR.

We discussed in section 2.4 that for 1D CGNR, we observed an angle dependent behaviour if we separate them as ZGNR and AGNR type CGNRs. What about CGNRs in 0D? Figure 3.7 (a) shows how energy levels of 0D CGNRs change with angle α. Figure 3.7 (b) shows how the HOMO-LUMO gap of 0D CGNRs changes with angle α for ten CGNRs we studied. By looking at these graphs, we can say that there can be a relationship between chiral angle α and the HOMO-LUMO gap of 0D CGNRs. If we include 0D ZGNRs as $\alpha = 0$CGNRs, the gap starts from 0eV, increases as alpha gets larger, and makes a peak around 12^o as 2.14eV, after which it drops slowly and goes below 0.16eV for $\alpha > 25^o$. The trend has a problem around 14^o. It occurs because the ribbon that is responsible for this point on the graph has a very long chiral vector $\vec{C}$ when it is compared with other ones around that angle. If we separate CGNRs into two different types

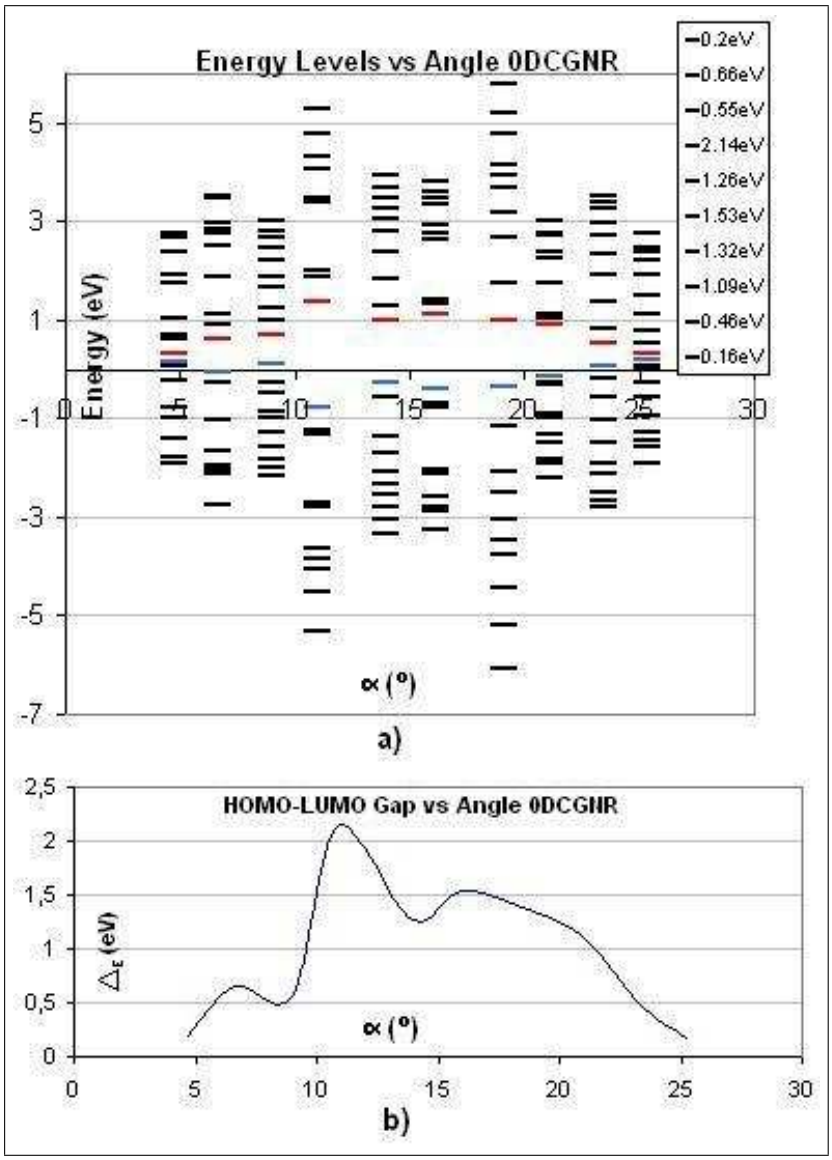

Figure 3.7: (a) Energy levels versus angle α. Blue lines represent HOMO levels and the red lines are for LUMO levels. (b) HOMO-LUMO gap versus angle α.

again, we can have a more meaningful result as shown in figure 3.8. In (a) we have a graph of HOMO-LUMO gap versus angle for ZGNR type 0D CGNR and in (b) HOMO-LUMO gap of AGNR type 0D CGNR. These graphs looks like a Gaussian distribution much more than the one both types included. Therefore, as in 1D CGNR case, two types of 0D CGNRs behave the same way but we still have to separate them.

$|\vec{C}|$ also has an important impact on the HOMO-LUMO gap values. Figure 3.9 (a) shows energy levels versus length of the chiral vector for all the ribbons we work with. The black lines are energy levels for the ribbons of ZGNR type,

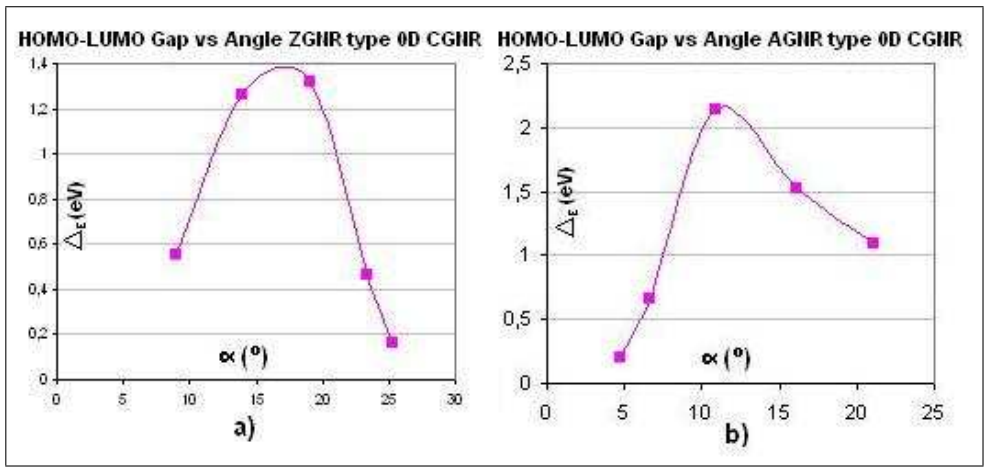

Figure 3.8: (a) HOMO-LUMO gap of ZGNR type 0D CGNRs versus angle. (b) HOMO-LUMO gap of AGNR type 0D CGNRs versus angle.

and the green lines are the energy levels for AGNR type 0D CGNRs. By looking at this figure, we cannot have a common sense about how the HOMO-LUMO gap depends on length of the chiral vector. However, if we make the same distinction for 0D CGNRs as we did for 1D CGNRs, we can see clearly that there is a dependence. Figure 3.9 (b) shows energy levels of ZGNR type CGNRs versus the length of chiral vector in 0D, and (c) shows energy levels of AGNR type CGNRs in 0D. Both of the figures show that there are HOMO-LUMO gaps for each type 0D CGNRs. However, these gaps decrease as we increase the length of the chiral vector. Also, just like the band gaps of AGNR type 1D CGNRs, AGNR type 0D CGNRs start from a higher HOMO-LUMO gap with respect to ZGNR type 0D

CGNRs, but drops much more quicker as we increase the length of $\vec{C}$. Therefore,

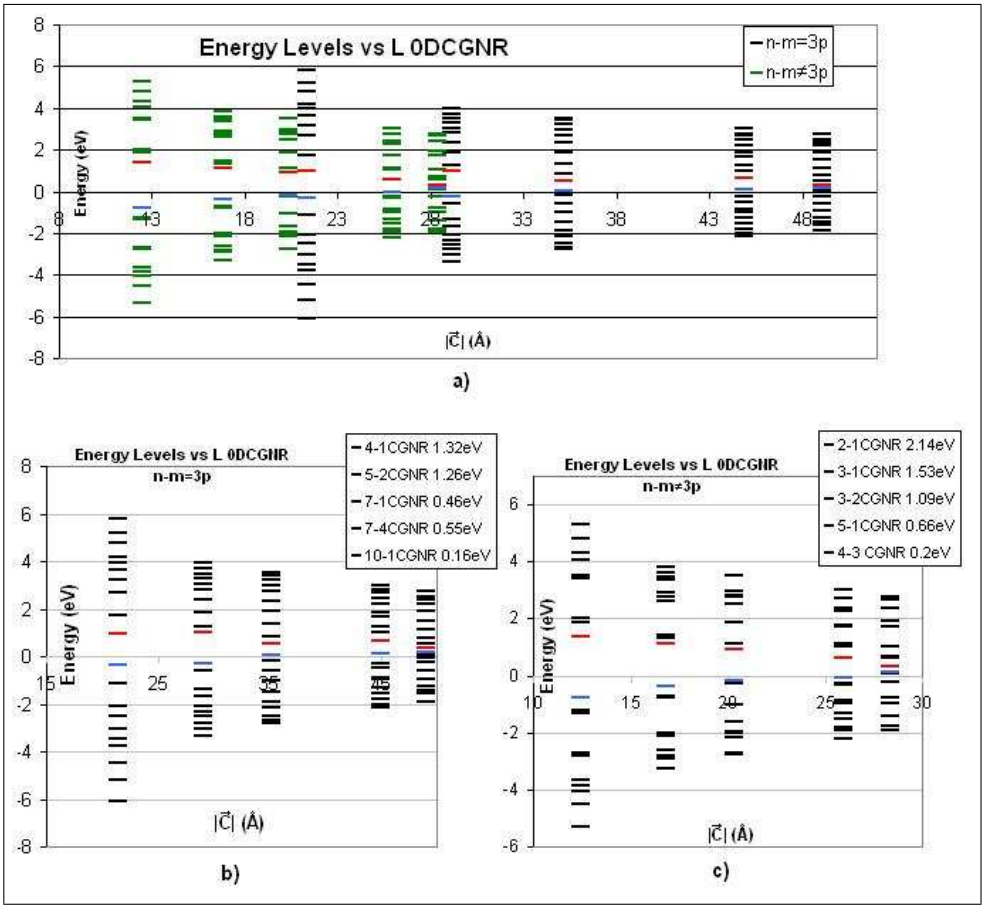

Figure 3.9: (a) Energy levels versus length of chiral vector for all 0D CGNRs. Green energy levels represent $n-m \neq 3p$, whereas, black lines stand for $n-m = 3p$, p being integer. (b) Energy levels versus length of $\vec{C}$ for ribbons having the property that $n-m$ is a multiple of three. (c) Energy levels versus length of $\vec{C}$ for the ribbons for which $n-m$ is not a multiple of three. In all graphs blue lines are HOMO and red lines are LUMO levels for that.

ZGNR type 0D CGNRs have noticeable HOMO-LUMO gaps even for $|\vec{C}| = 45$ Å($\Delta_E = 0.55eV$), whereas, AGNR type 0D CGNRs drops to 0.2eV for $|\vec{C}| = 28.3$ Å.

In conclusion, the electronic structure of 0D CGNRs has similarities to 1D CGNRs. 0D CGNRs can be divided into two families as ZGNR type and AGNR type 0D CGNRs. Both of the families have noticeable HOMO-LUMO gaps,

decreasing with the increase in the length of chiral vector $\vec{C}$. Both of the families show a Gaussian like distribution for the HOMO-LUMO gap as we increase the angle of chirality. 1D CGNRs have all these properties as well.

Chapter 4

Conclusions

In this work we presented the electronic band structures of one dimensional and zero dimensional graphene nano-ribbons. In 1D, zigzag graphene nano-ribbons show metallic behaviour, as the valance and conduction bands touch each other between K and M points. For 1D armchair graphene nano-ribbons however, there are two main groups. First one is $3N + 2$ group, in which all members show a metallic behaviour as we have zero band gap at Γ point. However, in the other group, all members show semiconducting behaviour. The band gap for this group members decreases as the width of the ribbon increases. For 1D chiral graphene nano-ribbons we see two distinct band structures which lets us call the ribbons as AGNR type CGNRs and ZGNR type CGNRs depending on the structure. In both of the families, there is band gap decreasing with the increase in width. These two families show the same behaviour independently as we change the chiral angle. The band gap starts from small values, reaches to a maximum and then, goes down to small values again as we change the angle between 0 and 30^o. In 0D, ZGNRs continue to show metallic behaviour whatever the length and width is. For 0D AGNRs, however, the width and length play a crucial role. For small AGNRs, we have noticeable band gaps. As we increase the width or the length, the band gap diminishes. In 0D AGNRs however, the two distinct groups cannot be observed as in 1D case. 0D CGNRs continue to show the same properties as if they are one dimensional. We still have two families

showing the same behaviour independently. As the length of the chiral vector increases, band gaps in both families decreases. Also, they seem to have similar band gap distribution with the change in angle just like they had in 1D case.

This work enables us to declare that AGNRs and (especially) CGNRs in both one and zero dimensions, can be used as semiconductors in applications. The calculations show that the smaller the ribbon is, the larger the band gap. Therefore, it is a strong candidate to replace silicon based transistors having a larger band gap as it's size gets smaller. The type, and size of the ribbon can be arranged by considering the band gaps and conditions that are presented.

There is still much work to be done in order to improve the quality of the calculations. The bond lengths that we assumed to be solid will not stay the same at the edges for both carbons and hydrogens [25]. Also there can be deformation in the structures for chiral graphene nano-ribbons due to the disordered shapes at the edges. Next thing to do is to examine how we can get rid of these problems. If we are able to do that, we can look forward to the changes in the band structures when we introduce impurities or defects [26].

Bibliography

[1] A. H. C. Neto, F. Guinea, N. M. R. Peres, K. S. Novoselov and A. K. Geim, arXiv:0709.1163, Rev. Mod. Phys. (to be published).

[2] K. S. Novoselov, A. K. Geim, S. V. Morozov, D. Jiang, Y. Zhang, S. V. Dubonos, I. V. Gregorieva, and A. A. Firsov, Science **306**, 666 (2004).

[3] Z. Chen, Y.-M. Lin, M. J. Rooks and P. Avouris, Physica E **40/2**, 228-232 (2007).

[4] M. Y. Han, B. Özyilmaz, Y. Zhang, and P. Kim, Phys Rev. Lett. **98**, 206805 (2007)

[5] G. Dresselhaus, M. S. Dresselhaus, and R. Saito, *Physical Properties of Carbon Nanotubes*, Imperial College Press, London, 1998.

[6] D. Tomanek, S. G. Louie, Phys. Rev B **37**, 8327 (1988).

[7] M. I. Katsnelson, Materials Today **10**, 1-2 (Jan-Feb 2007).

[8] P. R. Wallace, Phys. Rev. **71**, 622 (1947).

[9] A. N. Andriotis, E. Richter, and M. Menon, Appl. Phys. Lett. **91**, 152105 (2007).

[10] L. Pisani, J. A. Chan, B. Montanari, and N. M. Harrison, Phys. Rev. B **75**, 064418 (2007).

[11] Y.-W Son, M. L. Cohen, and S. G. Louie, Phys. Rev. Lett. **97**, 216803 (2006).

[12] E.-J Kan, Z. Li, J. Yang, and J. G. Hou, Appl. Phys. Lett. **91**, 243116 (2007).

[13] L. A. Agapito, and H.-P Cheng, J.Phys.Chem. C **111**, 14266-14273 (2007).

[14] H. Zheng, Z. F. Wang, T. Luo, Q. W. Shi, and J. Chen, Phys. Rev. B **75**, 165414 (2007).

[15] J. X. Cao, X. H. Yan, J. W. Ding, D. L. Wang, and D. Lu, J. Phys. Soc. Jpn. **71**, 5 (May 2002).

[16] L. Laaksonen, F. Muller-Plathe, and G. H. F. Diercksen, J. Chem. Phys **89**, 8 (15 October 1988).

[17] A. Rauk, *Orbital Interaction Theory of Organic Chemistry*, Pg.42, John Wiley and Sons, Inc. Canada, 1994.

[18] Brian Webster, *Chemical Bonding Theory*, Pg.178, Blackwell Scientific Publications, London, 1990.

[19] N.W. Alcock, *Bonding and Structure Structural Principles in Inorganic and Organic Chemistry*, Pg.112, Ellis Horwood Limited, England, 1990.

[20] R. V. Kasowski, Phys. Rev. Lett. **37**, 4, (26 July 1976).

[21] D. Finkenstadt, G. Pennington, and M. J. Mehl, Phys. Rev. B **76**,

121405(R) (2007).

[22] K. Tanaka, T. Sato, and T. Yamabe, Chem. Phys. Lett. **223**, 1-2, 10 Jun. 1994.

[23] Teri Wang Odom, Jin-Lin Huang, Philip Kim and Charles M. Lieber, J.Phys.Chem B **104**, 2794-2809 (2000).

[24] K. Grove-Rasmussen, and T. Jorgensen, *Electrical Properties of Carbon Nanotubes*, Bachelor thesis, Niels Bohr Institute (2000).

[25] S. Okada, Phys. Rev. B **77**, 041408(R) (2008).

[26] R. N. C. Filho, G. A. Farias, and F. M. Peeters, Phys. Rev. B **76**, 193409 (2007). [27] P. Shemella, Y. Zhang, M. Mailman, P. M. Ajayan, and S. K. Nayak, Appl. Phys. Lett. **91**, 042101 (2007).

[28] O. Hod, J. E. Peralta, and G. E. Scuseria, Phys. Rev. B **76**, 233401 (2007).

[29] V. I. Fal'ko and A. K. Geim, Eur. Phys. J. Special Topics **148**, 1-4 (2007).

[30] K. Nomura, and A. H. MacDonald, Phys. Rev. Lett. **98**, 076602 (2007).

[31] J.-C. Charlier, P. C. Eklund, J. Zhu, A. C. Ferrari, Topics Appl. Phys. **111**, 673-709 (2008).

[32] K. S. Novoselov, A. K. Geim, S. V. Morozov, D. Jiang, M. I. Katsnelson, I. V. Grigorieva, S. V. Dubonos, and A. A. Firsov, Nature **438**, 04233, (10 November 2005).

[33] A. K. Geim, and K. S. Novoselov, The Rise of Graphene, Nature

Mater. **6**, March 2007.

[34] J.-C. Charlier, Ph. Lambin, T. W. Ebbesen, Phys. Rev. B **54**, R8377 (1996).